

Subdiffusive dynamics and critical quantum correlations in a disorder-free localized Kitaev honeycomb model out of equilibrium

Guo-Yi Zhu* and Markus Heyl

Max Planck Institute for the Physics of Complex Systems, Nöthnitzer Straße 38, Dresden 01187, Germany
(Dated: September 21, 2021)

Disorder-free localization has recently emerged as a mechanism for ergodicity breaking in homogeneous lattice gauge theories. In this work we show that this mechanism can lead to unconventional states of quantum matter as the absence of thermalization lifts constraints imposed by equilibrium statistical physics. We study a Kitaev honeycomb model in a skew magnetic field subject to a quantum quench from a fully polarized initial product state and observe nonergodic dynamics as a consequence of disorder-free localization. We find that the system exhibits a subballistic power-law entanglement growth and quantum correlation spreading, which is otherwise typically associated with thermalizing systems. In the asymptotic steady state the Kitaev model develops volume-law entanglement and power-law decaying dimer quantum correlations even at a finite energy density. Our work sheds light onto the potential for disorder-free localized lattice gauge theories to realize quantum states in two dimensions with properties beyond what is possible in an equilibrium context.

I. INTRODUCTION

It is the general expectation that realistic isolated quantum many-body systems driven out of equilibrium eventually thermalize such that the relaxed long-time steady states become locally indistinguishable from thermal ensembles [1–6]. Two types of celebrated exceptions beyond this paradigm are quantum integrable models [7–11] and the Anderson or many-body localization (MBL) mechanism imposed by strong disorder [12, 13]. In two dimensions, the exploration of ergodicity breaking dynamics in interacting systems remains a challenge especially in view of the argued instability of MBL in two dimensions [14]. Recent years have witnessed a new type of mechanism for nonergodic dynamics unique to lattice gauge theories where static local gauge charge or flux serves as a source for an effective internal disorder [15–17]. Importantly, this so-called disorder-free localization scenario does not rely on breaking translational invariance and can even occur in interacting two dimensional models [18, 19], opening up a promising route targeting the challenge of realizing quantum states in two dimensional nonergodic systems with properties beyond any equilibrium counterpart.

In this work we show that the Kitaev honeycomb model driven to highly-excited states by a nonequilibrium quantum quench enters a peculiar disorder-free localized phase exhibiting subdiffusive dynamics towards a critical state exhibiting an algebraically decaying dimer quantum correlation function. Specifically, we investigate the nonequilibrium dynamics in the Kitaev honeycomb model in a weak skew magnetic field starting from a spin polarized initial state. The problem can be mapped to a weakly interacting Majorana fermion model coupled to a static \mathbb{Z}_2 gauge field [20], which for the considered dynamics becomes effectively disordered.

Although a number of previous works have considered the intertwined physics between fermion and flux in the Kitaev model [21–29], the central open question has remained as to whether this model can break ergodicity and can potentially host non-thermal quantum order. In the noninteracting limit, we find that the gauge flux disorder localizes most of the Majorana fermions but fails to freeze the metallic and critical modes, leading to the observed subdiffusive dynamics although the system is overall nonergodic [30–34]. We identify the subdiffusive dynamics in both an algebraic spread of quantum correlations and the power-law growth of entanglement. At late times, the system relaxes to a steady state with dimer quantum correlation functions decaying algebraically in space, which is characteristic of quasi-long range order not accessible in thermal equilibrium. We argue that this quasi-long range order implies a divergent multipartite entanglement as quantified by the quantum Fisher information. We find evidence that our main findings are robust against the leading order perturbative Majorana fermion interactions induced by the skew magnetic field according to our numerical calculations for up to 128 spins on long time scales. Our results can be extended to any \mathbb{Z}_2 lattice gauge theory coupled to chiral Majorana fermions as long as the gauge flux can be considered static and disordered on the considered time scales.

II. MODEL

The Kitaev model consists of spin- $\frac{1}{2}$ degrees of freedom on the honeycomb lattice with spin-orbital locking Ising interactions $D_j^\mu = -\sigma_j^\mu \sigma_{j+e_\mu}^\mu$, where j labels spin site and e_μ denotes nearest neighbour vector of different orientations $\mu = x, y, z$ (Fig. 1a). In the presence of a weak [111] skew magnetic field the Hamiltonian is

$$\hat{H}_K = \sum_j \sum_{\mu=x,y,z} \left(J_\mu \sigma_j^\mu \sigma_{j+e_\mu}^\mu + h \sigma_j^\mu \right), \quad h \ll J_\mu. \quad (1)$$

* timeexplorer1991@gmail.com

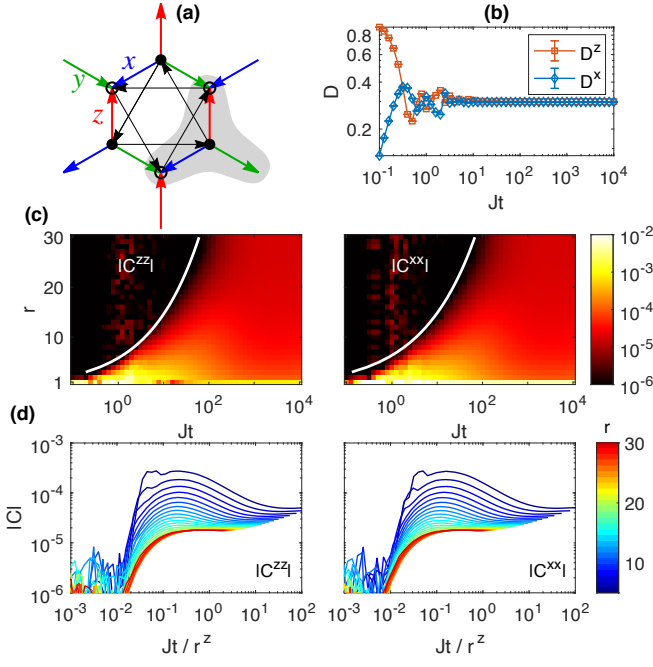


FIG. 1. (a) Model interactions. Arrows indicate Majorana fermion hopping. Four Majorana fermions interact within every Y junction, shaded in gray. (b) $\langle D^{z(x)}(t) \rangle$. (c) $C^{\mu\mu} = \langle D_j^\mu D_{j+r}^\mu \rangle_c$. The propagating wave-front is determined by threshold $|C| \geq 10^{-6}$, subject to a power-law fitting $r \propto (Jt)^{1/z}$ indicated by white lines. $z = 2.5(2)$ for $|C^{zz}|$ and $z = 2.7(3)$ for $|C^{xx}|$. (d) Collapse of correlation growth at fixed distance with rescaled time. The parameters are $J_z = J_x = J_y = J, \tilde{h} = 0.25J$, 10000 disorder samples of system size with 60×60 unit cells (7200 spins).

For $h = 0$ the product $\hat{W} \equiv D^x D^y D^z D^x D^y D^z$ surrounding a hexagon plaquette commutes with \hat{H}_K , implying an extensive number of local integrals of motion. In the targeted limit $h \ll J_\mu$ we take into account the magnetic field perturbatively to the leading order that preserves these local symmetries [20]:

$$\hat{H} = \sum_{\mu} \sum_j J_{\mu} \sigma_j^{\mu} \sigma_{j+e_{\mu}}^{\mu} + \tilde{h} \sum_{(ijk) \in \Lambda, Y} \sigma_i^x \sigma_j^y \sigma_k^z, \quad (2)$$

where $\tilde{h} \propto h^3/J^2$. The perturbative interaction acts on three spins that live on any wedges \wedge , or the end of any Y junction. Either by introducing the gauge redundancy [20] and fixing the gauge, or by a Jordan-Wigner transformation [35, 36], one can map \hat{H} onto an interacting Majorana fermion minimally coupled with \mathbb{Z}_2 gauge field on the links:

$$\hat{H} = \sum_{\langle j \rightarrow l \rangle} J_{\mu} i u_{j,l} \beta_j \alpha_l + \tilde{h} \sum_{\langle\langle j \rightarrow l \rangle\rangle} i u_{j,k} u_{k,l} (\alpha_j \alpha_l + \beta_j \beta_l) + \tilde{h} \sum_Y u_{i,j} u_{i,k} u_{i,l} (\beta_i \alpha_j \alpha_k \alpha_l - \alpha_i \beta_j \beta_k \beta_l), \quad (3)$$

where $\alpha(\beta)$ denotes Majorana fermion on $A(B)$ sublattice marked with open(close) circle in Fig. 1a. The static

gauge field on link is pinned to $u_{j,j-e_x(y)} = 1$, $u_{j,j-e_z} = \pm 1$. \hat{W} on plaquettes are transformed to be locally conserved \mathbb{Z}_2 gauge fluxes. The last four fermion term is a chiral and gauged Majorana Hubbard interaction [37], where j, k, l are arranged in a counter-clockwise order around i .

III. QUANTUM QUENCH PROTOCOL

We prepare a simple initial state as a Néel state such that $\sigma^z |\Psi_0\rangle = \pm |\Psi_0\rangle$ on A/B sublattice respectively, which is to be evolved by \hat{H} later on. In the fermion representation the initial state becomes a gauged fermion vacuum coupled to a disordered gauge field background:

$$|\Psi(t)\rangle = \frac{1}{2^{N/2}} \sum_{\{u\}} e^{-it\hat{H}_{\{u\}}} |\{u\}\rangle \otimes |\psi_{\{u\}}\rangle, \quad (4)$$

where N is the number of unit cells (z -links), and the Fock state satisfies $i u_{j,j-e_z} \alpha_j \beta_{j-e_z} |\psi_{\{u\}}\rangle = |\psi_{\{u\}}\rangle$. In the sector $\prod_j \sigma_j^z = 1$ the anti-periodic boundary condition in spin Hamiltonian is mapped to periodic boundary in Majorana Hamiltonian. In this main-text we'll mainly focus on the isotropic coupling $J_x = J_y = J_z \equiv J, \tilde{h} = 0.25J$.

For observables that preserve the gauge field $\hat{O} = \sum_{\{u\}} O_{\{u\}}$ [15, 16],

$$\langle \Psi_0 | \hat{O}(t) | \Psi_0 \rangle = \frac{1}{2^N} \sum_{\{u\}} \langle \psi_{\{u\}} | e^{it\hat{H}_{\{u\}}} \hat{O}_{\{u\}} e^{-it\hat{H}_{\{u\}}} | \psi_{\{u\}} \rangle, \quad (5)$$

where the average over gauge-field configurations can be performed via Monte-Carlo sampling. The typical $\{u\}$ configuration is random, making the dynamical problem equivalent to Majorana fermions subject to \mathbb{Z}_2 gauge (π) flux disorder, although our model is overall translational invariant [15, 16].

Overall we target the description of the nonequilibrium dynamics through a sequence of two steps. First, we will study in detail the exact solvable point i.e. the noninteracting limit of Eq. (3), where we find that the system becomes nonergodic due to disorder-free localization, and afterwards explore the influence of interactions.

IV. EXACTLY SOLVABLE POINT

When the Majorana interactions are neglected, the model becomes exactly solvable. For each gauge configuration the dynamics is governed by a free Majorana fermion Gaussian Hamiltonian that can be computed efficiently. By randomly sampling gauge fields $u = \pm 1$ on the z -links, we compute the real-time evolution of various physical observables that are natural in both the spin and the fermion language.

First, we consider the spin dimer expectation values $D_j^\mu = i u_{j,j-e_\mu} \alpha_j \beta_{j-e_\mu}$ ($\mu = z, x$), which relax exponentially fast to the same constant losing the memory of

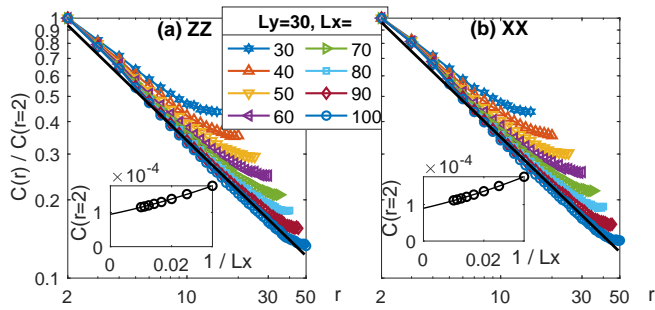


FIG. 2. Dimer correlations in the steady state, averaged over $10^{3.6} \lesssim Jt \lesssim 10^4$. Black lines indicate power-law fitting $r^{-\Delta}$ with $\Delta = 0.63(2)$ for both C^{zz} and C^{xx} . Insets show correlations at $r = 2$ extrapolated to finite value in thermodynamic limit.

initial anisotropy (see Fig. 1b). The observables along x and y directions can be related by mirror symmetry. As we will show, the dimer quantum correlation functions $C^{zz(xx)}(r, t) = \frac{1}{N} \sum_j \langle \Psi(t) | D_j^{z(x)} D_{j+r}^{z(x)} | \Psi(t) \rangle_c$, exhibit a much slower and intricate dynamics, which quantifies the correlation of gauged local fermion parity. Remarkably, we find that $C^{zz(xx)}(r, t)$ exhibits an algebraic light-cone in spacetime, see Fig. 1(c), with the wave-front following a power-law $Jt \propto r^z$ behavior. The dynamical exponent is obtained as $z = 2.5(2)$ for $|C^{zz}|$ while $z = 2.7(3)$ for $|C^{xx}|$. Notice that the dynamical exponent z here is associated with information transport instead of particle or energy transport, and $z > 1$ signals subdiffusion [38]. In Fig. 1d we further corroborate this by achieving a data collapse upon rescaling the time axis Jt/r^z . While such subballistic behavior in systems with conventional disorder is typically observed on the ergodic side close to the MBL transition lying between diffusive and glassy limit [30–34], here we observe such dynamics for a disorder-free localized model, as we will argue in more detail below.

At long times the system settles to a steady state, which, as we find, is of nonergodic critical nature with correlations decaying algebraically in space, as seen in Fig. 2. We observe that the decay of $C^{zz(xx)}(r, t)$ is consistent with a power-law in space, whose exponent increases for larger system sizes and appears to converge near $0.63(2)$. The power-law decaying correlation function in all directions x, y, z are reminiscent of the Kosterlitz-Thouless phase with quasi-long range order [39], without spontaneously breaking the spin-orbital three-fold rotation symmetry. However, even when this symmetry is explicitly broken in the anisotropic regime, we still observe critical correlation [40]. It is the effective disorder that partially inhibits the finite energy density fluctuations and stabilizes the quasi-long range spin dimer order [41].

These critical quantum correlations further have an immediate impact onto the entanglement content of the reached steady state, as the dimer quantum correlation function can be directly linked to a quantum Fisher infor-

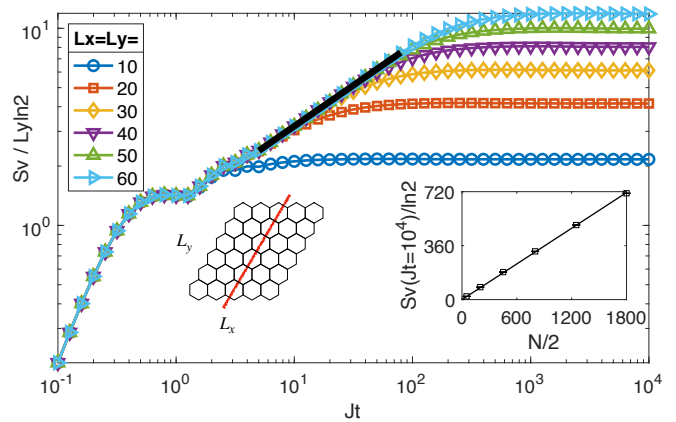


FIG. 3. Projective bipartite entanglement entropy, averaged over 1000 disorder samples. The inset shows the entanglement cut. The black line indicates the power-law fitting $\propto t^{1/z}$ with $z = 2.4(1)$. At late time, entropy saturates to a volume law $S_v(Jt = 10^4) = 0.40(1)N \ln 2/2$, as shown in the inset.

mation density via $f_Q^{zz(xx)}(t) = \sum_r C^{zz(xx)}(r, t)$ [42–44]. Since $C^{zz(xx)}(r, t) \sim r^{-\Delta}$ with $0 < \Delta < 1$ for $t \rightarrow \infty$ we find that $f_Q^{zz(xx)} \sim N^{1-\Delta}$ diverges in the thermodynamic limit. As a consequence the steady state exhibits strong multipartite entanglement.

For a more detailed quantification of the entanglement properties we further consider the projective bipartite entanglement entropy that serves as an entanglement diagnostics for quantum disentangled liquids [45–47]. Namely, we measure the von Neumann entanglement entropy for half of the Majorana fermions, when the gauge field is projected onto the diagonal ensemble:

$$S_v = \frac{1}{2N} \sum_{\{u\}} S_{\{u\}}, \quad S_{\{u\}} = -\hat{\rho}_{\{u\}} \ln \hat{\rho}_{\{u\}}, \quad (6)$$

with the reduced density matrix

$$\hat{\rho}_{\{u\}} = \text{Tr}_{\alpha, \beta \in L} e^{-it\hat{H}_{\{u\}}} |\psi_{\{u\}}\rangle \langle \psi_{\{u\}}| e^{it\hat{H}_{\{u\}}} \quad (7)$$

obtained from tracing out Majorana fermions on the left half of the lattice (see inset in Fig. 3). $\hat{\rho}_{\{u\}}$ is a Gaussian operator which can be computed exactly [48, 49]. Note that while we can compute local observables and correlation functions exactly, the non-projective von Neumann entropy of the Kitaev model is not diagonal with respect to the gauge configurations and therefore cannot be reduced to a free fermion problem, unlike the low order Renyi entropy [50]. Diagonal entanglement entropies such as the one we consider have been used already for localized systems in other contexts [51] and give an upper bound on the actual entanglement entropy [52]. As shown in Fig. 3, at early time the entanglement grows with an area law. At a second stage, the entanglement entropy exhibits a further growth according to a subballistic power-law $S \propto t^z$. From a fit to the data we obtain the entanglement dynamical exponent $z = 2.4(1)$,

which within the accuracy of our simulations aligns with the exponent appearing for the subballistic spreading in $C^{zz}(xx)(r,t)$. In a system of finite size, we find that the entanglement entropy saturates to a volume-law state $S_v \propto L_x L_y$ typical for the highly excited free fermion states [53, 54], as shown in inset of Fig. 3. These numerical findings again highlight the unconventional nonequilibrium dynamics that we observe in the disorder-free localized Kitaev model.

One may ask what if we deform the initial state. By tuning the gauge flux density in the initial state by applying an operator $\prod_q (\frac{1}{2} + (\frac{1}{2} - p)\hat{W}_q)$, the exponent Δ as well as z change continuously, as visible in Fig. 4, which corroborates the robustness of the critical dynamical phase reminiscent of Kosterlitz-Thouless phase. However, notice that our critical dynamical phase at late-time steady state should be contrasted with the one exhibiting critical initial slip in short-time relaxation [55].

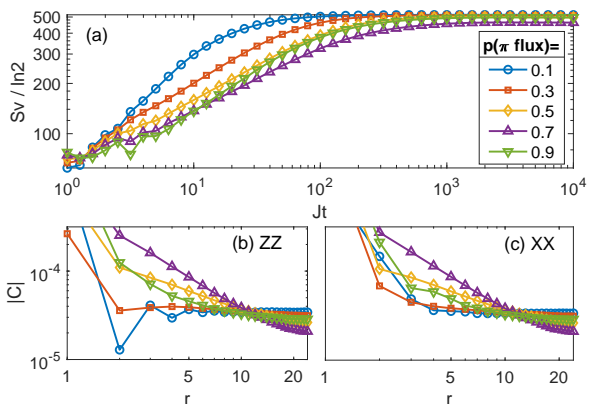


FIG. 4. Tuning the density of π fluxes. (a) projective bipartite entanglement entropy of Majorana fermions. (b)(c) Steady state spatial correlation function $|C^{zz}(xx)|$, averaged in the time window $10^3 \lesssim Jt \lesssim 10^4$. The parameters are $J_z = J_x = J_y \equiv J, \hbar = 0.25J, L_x = L_y = 50$, 1000 disorder samples.

V. LOCALIZATION ANALYSIS

The peculiar coexistence of subdiffusive dynamics at transient time and the quasi-long-range order at late time implies a subtle localization scenario in behind. Indeed we find a mixture of localized and critical modes from the standard numerical diagnostics [40] including level spacing statistics [56, 57], localization length in two dimensions [58–60], and Chern number [20, 61–63].

The localization length is calculated by the retarded Green’s function using iterative Dyson’s equation for a semi-infinite quasi-one-dimensional geometry, followed by a one-parameter-scaling-collapse for varying narrow width. As shown in Fig. 5a, the localization length and the level spacing ratio for a finite size system are consistent in showing three energy windows with delocalization tendency. The delocalization at zero energy was

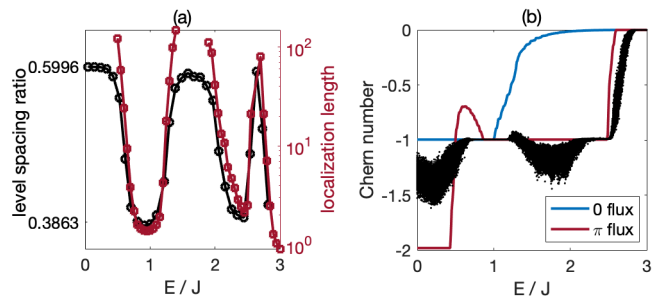


FIG. 5. (a) The left axis shows the level spacing ratio, for system size $L_x = L_y = 60$ with 10000 disorder samples. The characteristic value for the Poisson ensemble $2 \ln 2 - 1 \simeq 0.3863$ and the one for Gaussian unitary ensemble ≈ 0.5996 are indicated. The right axis shows the localization length obtained by one-parameter scaling for a sequence of quasi-1D long stripes for $L_y = 8, 16, 32, 64, 128$, and $L_x \leq 10^6$. (b) Chern number for system size $L_x = L_y = 40$. Black dots are for 500 disorder samples, while the blue(red) line is for the zero(π) flux clean system.

known to be responsible for a low-energy Majorana thermal metal state in the class D dirty superconductors [64–66] or Majorana lattice model [67–69], which entails logarithmic divergent density of states and weak multi-fractal nature as we numerically verify [40, 70]. Intuitively, the low-energy delocalized Majorana mode arises from percolating through an extensive number of resonating Majorana zero modes trapped in \mathbb{Z}_2 gauge fluxes in a weak pairing topological superconductor [68, 71].

To gain more insight into the topology of the fermion, we calculate the Chern number of the fermion eigenstates [72–74] of varying energy by using the real-space formula based on concept of non-commutative Brillouin zone:

$$C = \frac{2\pi i}{N} \text{Tr}([P_x P, P_y P]), \quad P(E) = \sum_{\epsilon < -E} |\epsilon\rangle\langle\epsilon|. \quad (8)$$

Here x, y are the real-space coordinate operators which label the first quantized orbitals and generate the translation of crystal momenta, $|\epsilon\rangle$ is the single-particle eigenstate of the first quantized Hamiltonian matrix with energy ϵ . $P(E)$ is the spectral projector where the single-particle mode with energy smaller than $-E$ is occupied, mimicking the Fermi level in the complex fermion system with number conservation. In a fermionic system with only fermion parity conservation, half of the single-particle eigenstates are redundant, so we consider only $E \geq 0$. The change of $C(E)$ reveals the Berry flux carried by the fermion mode at the corresponding energy. From Fig. 5b, the delocalized mode near $E \simeq 2.5(1)J$ is clearly associated with a topological quantum critical point separating two distinct Chern plateaus, that is robust against perturbation and weak disorder [75, 76]. As for the energy window $1.5J \lesssim E \lesssim 2.0J$, it is unclear whether it would maintain a finite mobility edge or shrink to a singular point or become fully localized in the thermodynamic limit [77, 78].

A final comment is that our result is consistent with the argument that non-Abelian topological phases cannot be fully localized [79]. While disorder tends towards localization, i.e., a divergent dynamical exponent $z \rightarrow \infty$, this tendency competes with the metallic and topology induced critical modes favoring ballistic propagation with $z = 1$, leading to the observed subdiffusive dynamics with $z > 1$.

VI. BEYOND EXACT SOLVABLE LIMIT

Now we aim to address the robustness of our observations upon the influence of interactions present in Eq. (3). Here, we will focus on the leading order resonant contributions responsible for an eventual destabilisation, by utilizing the approach introduced in Ref. [80], where it has been shown that these resonant contributions can capture the essential non-perturbative effects of interactions such as the logarithmic entanglement growth in MBL phases not only on a qualitative but also on a quantitative level. The Hamiltonian is then expressed in the canonical fermion basis

$$\hat{H}_\gamma = - \sum_{n=1}^N \epsilon_n i \gamma'_n \gamma''_n - \frac{1}{4} \sum_{m,n=1}^N V_{m,n} \gamma'_m \gamma''_m \gamma'_n \gamma''_n + \dots, \quad (9)$$

where the canonical Majorana fermions γ' , γ'' are related to the original local Majorana fermions by an orthogonal transformation obtained from diagonalizing the non-interacting fermion part. The leading order resonant interaction preserves the parity of the canonical fermion mode $\langle i \gamma'_n \gamma''_n \rangle$ but induces a dephasing effect, analogous to the l -bit theory in MBL systems [12, 13] in which it leads to dramatic non-perturbative effect [80]. In our case of Kitaev model with weak magnetic field, we also find a special structure for this interaction strength $V_{m,n}$, which endows a hierarchy of dephasing timescales (see Fig. 6a). It is the key observation in Ref. [80] that the dynamics of any fermion correlation function can be effectively written as a sum over a number $O(N^4)$ of Gaussian evolution trajectories, schematically abbreviated as

$$\langle \psi(t) | \gamma_m \gamma_n \gamma_p \gamma_q | \psi(t) \rangle = \sum_{mnpq} C \langle \psi | e^{-it \frac{1}{4} \gamma A_{mnpq} \gamma} \gamma_m \gamma_n \gamma_p \gamma_q | \psi \rangle, \quad (10)$$

which can be further factorized into the product of a Loschmidt amplitude quantity and an effective correlation function [40, 81–85]. As shown in Fig. 6d, we calculate the system with 16×4 unit cells (128 spins) up to the timescale $Jt \leq 10^4$, where the interacting scenario turns out to collapse with the non-interacting case within numerical accuracy. The critical quantum correlations are therefore stable up to this timescale. We estimate the validity of the perturbative approach by statistics of resonances in first-order perturbation theory of the omitted terms. We find that they are off-resonant with probability $\gtrsim 99.5\%$ for the considered parameter regime [40], above typical thresholds [86], so that they can become

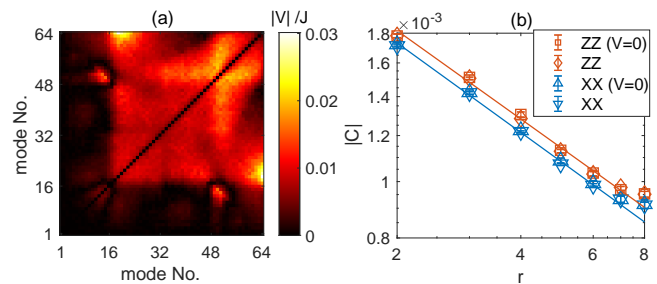


FIG. 6. (a) V_{mn} . The mode index corresponds to the energy in ascending order. (b) Correlation functions of steady state, averaged in time window $10^3 \lesssim Jt \lesssim 10^4$. The power-law-fitting exponent is $0.50(6)$ for C^{zz} , and $0.51(4)$ for C^{xx} . The parameters are $\tilde{h} = 0.25J$, $L_x = 16$, $L_y = 4$, 200 disorder samples. The $V = 0$ case for comparison takes 10000 disorder samples.

relevant only via higher-order processes manifesting on longer timescales.

VII. CONCLUDING DISCUSSION

While thermalization may occur eventually for the full Hamiltonian in Eq. (1) on long time scales, we emphasize that our findings imply a long intermediate time window with nonergodic behavior leading to exotic quantum dynamics and correlations. On the other hand, it is tempting to ask whether the exotic dynamics and non-equilibrium quantum order are related to the low-energy non-Abelian Ising topological order [20, 87]. However, in the strongly anisotropic coupling regime which in zero temperature exhibit a distinct Abelian \mathbb{Z}_2 topological order [88], we find similar high energy critical mode and subdiffusive dynamics as well as critical correlation, which goes beyond the low energy universality class [40]. Our findings of subdiffusive dynamics and critical quantum correlations may emerge universally in general \mathbb{Z}_2 lattice gauge theories coupled to chiral Majorana matter fermions, provided two essential ingredients: (i) nontrivial fermion topology; (ii) static disordered gauge flux [89–92]. Above all, our observation of quasi-long range order with associated divergent multipartite entanglement in a non-equilibrium high-energy steady state marks a concrete first step towards yet unexplored unconventional phase structures in ergodicity breaking two dimensional quantum models. Subdiffusion might be present also in a more general context of Majorana spin liquids as long as the effective \mathbb{Z}_2 gauge flux (vison) dynamics is much slower than that of the fermions, which will be a challenging but valuable scope for future research. Furthermore, motivated by the recent developments showing that the gauge charge disorder in a 1D unconstrained gauge theories can stabilize a time crystal order [93], it would also be interesting to generalize this idea to two dimensions in search of nontrivial spatiotemporal order from a driven Kitaev model [94, 95]. Finally, beyond the

conceptual interest, the nonequilibrium quench dynamics can in principle be realized in various quantum architectures including ultracold atoms [96, 97], superconducting qubits [98, 99] or topological nanowires [100, 101], as well as via ultrafast pump-probe techniques in the Kitaev candidate materials at sufficiently low temperatures with suppressed phonon influence [29, 102–106].

ACKNOWLEDGMENTS

Acknowledgments.— The authors would like to thank G. D. Tomasi, C. Castelnovo and O. Hart for helpful dis-

cussions. G.-Y. Zhu also thanks S.-K. Jian and C. Chen for inspiring discussions, and the IT teams in MPIPKS and MPCDF for the technical support in computations. This project has received funding from the European Research Council (ERC) under the European Union’s Horizon 2020 research and innovation programme (grant agreement No. 853443), and M. H. further acknowledges support by the Deutsche Forschungsgemeinschaft (DFG) via the Gottfried Wilhelm Leibniz Prize program.

-
- [1] J. M. Deutsch, Quantum statistical mechanics in a closed system, *Physical Review A* **43**, 2046 (1991).
 - [2] M. Srednicki, Chaos and quantum thermalization, *Physical Review E* **50**, 888 (1994).
 - [3] M. Rigol, V. Dunjko, and M. Olshanii, Thermalization and its mechanism for generic isolated quantum systems, *Nature* **452**, 854 (2008), 0708.1324v2.
 - [4] J. Eisert, M. Friesdorf, and C. Gogolin, Quantum many-body systems out of equilibrium, *Nature Physics* **11**, 124 (2015), 1408.5148v2.
 - [5] J. M. Deutsch, Eigenstate thermalization hypothesis, *Reports on Progress in Physics* **81**, 082001 (2018), 1805.01616v1.
 - [6] A. Mitra, Quantum quench dynamics, *Annual Review of Condensed Matter Physics* **9**, 245 (2018), 1703.09740v2.
 - [7] P. Calabrese and J. Cardy, Evolution of entanglement entropy in one-dimensional systems, *Journal of Statistical Mechanics: Theory and Experiment* **2005**, P04010 (2005), cond-mat/0503393v1.
 - [8] P. Calabrese and J. Cardy, Time-dependence of correlation functions following a quantum quench, *Physical Review Letters* **96**, 136801 (2006), cond-mat/0601225v2.
 - [9] V. Alba and P. Calabrese, Entanglement and thermodynamics after a quantum quench in integrable systems, *Proceedings of the National Academy of Sciences* **114**, 7947 (2017), 1608.00614v2.
 - [10] J. E. Moore, A perspective on quantum integrability in many-body-localized and yang–baxter systems, *Philosophical Transactions of the Royal Society A: Mathematical, Physical and Engineering Sciences* **375**, 20160429 (2017).
 - [11] P. Calabrese, Entanglement spreading in non-equilibrium integrable systems, *SciPost Phys. Lect. Notes* , 20 (2020).
 - [12] R. Nandkishore and D. A. Huse, Many body localization and thermalization in quantum statistical mechanics, *Annual Review of Condensed Matter Physics* **6**, 15 (2015), 1404.0686v2.
 - [13] D. A. Abanin, E. Altman, I. Bloch, and M. Serbyn, Many-body localization, thermalization, and entanglement, *Reviews of Modern Physics* **91**, 021001 (2019), 1804.11065v2.
 - [14] I.-D. Potirniche, S. Banerjee, and E. Altman, On the stability of many-body localization in $d > 1$, *Physical Review B* **99**, 205149 (2019), 1805.01475.
 - [15] A. Smith, J. Knolle, D. L. Kovrizhin, and R. Moessner, Disorder-free localization, *Physical Review Letters* **118**, 266601 (2017), 1701.04748v2.
 - [16] M. Brenes, M. Dalmonte, M. Heyl, and A. Scardicchio, Many-body localization dynamics from gauge invariance, *Physical Review Letters* **120**, 030601 (2018), 1706.05878v2.
 - [17] H. Yarloo, A. Langari, and A. Vaezi, Anyonic self-induced disorder in a stabilizer code: quasi-many body localization in a translational invariant model, *Physical Review B* **97**, 054304 (2018), 1703.06621.
 - [18] A. Smith, J. Knolle, R. Moessner, and D. L. Kovrizhin, Dynamical localization in \mathbb{Z}_2 lattice gauge theories, *Physical Review B* **97**, 245137, 1803.06574.
 - [19] P. Karpov, R. Verdel, Y. P. Huang, M. Schmitt, and M. Heyl, Disorder-free localization in an interacting two-dimensional lattice gauge theory, 2003.04901v1.
 - [20] A. Kitaev, Anyons in an exactly solved model and beyond, *Annals of Physics* **321**, 2 (2006), cond-mat/0506438v3.
 - [21] J. Knolle, D. L. Kovrizhin, J. T. Chalker, and R. Moessner, Dynamics of a two-dimensional quantum spin liquid: signatures of emergent majorana fermions and fluxes, *Physical Review Letters* **112**, 207203 (2014), 1308.4336.
 - [22] X.-Y. Song, Y.-Z. You, and L. Balents, Low-energy spin dynamics of the honeycomb spin liquid beyond the kitaev limit, *Physical Review Letters* **117**, 037209 (2016), 1604.04365.
 - [23] J. Nasu, J. Yoshitake, and Y. Motome, Thermal transport in the kitaev model, *Physical Review Letters* **119**, 127204 (2017), 1703.10395v1.
 - [24] A. Metavitsiadis, A. Pidotella, and W. Brenig, Thermal transport in a two-dimensional \mathbb{Z}_2 spin liquid, *Physical Review B* **96**, 205121 (2017), 1707.03836v1.
 - [25] M. Gohlke, R. Moessner, and F. Pollmann, Dynamical and topological properties of the kitaev model in a [111] magnetic field, *Physical Review B* **98**, 014418 (2018), 1804.06811v2.
 - [26] J. Knolle, S. Bhattacharjee, and R. Moessner, Dynamics of a quantum spin liquid beyond integrability – the kitaev-heisenberg- γ model in an augmented parton mean-field theory, *Physical Review B* **97**, 134432, 1801.03774v1.

- [27] M. Gohlke, R. Verresen, R. Moessner, and F. Pollmann, Dynamics of the kitaev-heisenberg model, *Physical Review Letters* **119**, 157203 (2017), 1701.04678v1.
- [28] L. Rademaker, Quenching the kitaev honeycomb model, *SciPost Physics* **7**, 071 (2019), 1710.09761v4.
- [29] J. Nasu and Y. Motome, Nonequilibrium majorana dynamics by quenching a magnetic field in kitaev spin liquids, *Physical Review Research* **1**, 033007 (2019), 1905.10984.
- [30] E. Altman and R. Vosk, Universal dynamics and renormalization in many body localized systems, *Annual Review of Condensed Matter Physics* **6**, 383 (2015), 1408.2834v1.
- [31] R. Vosk, D. A. Huse, and E. Altman, Theory of the many-body localization transition in one dimensional systems, *Physical Review X* **5**, 031032 (2015), 1412.3117v2.
- [32] D. J. Luitz, N. Laflorencie, and F. Alet, Extended slow dynamical regime close to the many-body localization transition, *Physical Review B* **93**, 060201 (2016), 1511.05141v2.
- [33] D. J. Luitz and Y. B. Lev, Information propagation in isolated quantum systems, *Physical Review B* **96**, 020406 (2017), 1702.03929v1.
- [34] T. L. M. Lezama and D. J. Luitz, Power-law entanglement growth from typical product states, *Physical Review Research* **1**, 033067 (2019), 1908.07010v2.
- [35] X.-Y. Feng, G.-M. Zhang, and T. Xiang, Topological characterization of quantum phase transitions in a $s=1/2$ spin model, *Physical Review Letters* **98**, 087204 (2007), cond-mat/0610626v1.
- [36] D.-H. Lee, G.-M. Zhang, and T. Xiang, Edge solitons of topological insulators and fractionalized quasiparticles in two dimensions, *Physical Review Letters* **99**, 196805 (2007), 0705.3499v2.
- [37] A. Rahmani and M. Franz, Interacting majorana fermions, *Reports on Progress in Physics* **82**, 084501 (2019), 1811.02593v1.
- [38] D. J. Luitz and Y. B. Lev, The ergodic side of the many-body localization transition, *Annalen der Physik* **529**, 1600350 (2017), 1610.08993.
- [39] J. M. Kosterlitz, The critical properties of the two-dimensional xy model, *Journal of Physics C: Solid State Physics* **7**, 1046 (1974).
- [40] See Supplemental Material for the numerical results and technical details for: dynamics of tuning flux density; other Majorana fermion correlations; the dynamics of anisotropic coupling case; time reversal symmetric case; the fermionization; deriving the time evolved physical observables with and without interaction; calculating localization length and Chern number; evidence of zero energy Majorana metallic state..
- [41] D. A. Huse, R. Nandkishore, V. Oganesyan, A. Pal, and S. L. Sondhi, Localization protected quantum order, *Physical Review B* **88**, 014206 (2013), 1304.1158v1.
- [42] P. Hyllus, W. Laskowski, R. Kirschke, C. Schwemmer, W. Wiczkorek, H. Weinfurter, L. Pezzé, and A. Smerzi, Fisher information and multiparticle entanglement, *Physical Review A* **85**, 022321 (2012), 1006.4366.
- [43] G. Toth, Multipartite entanglement and high precision metrology, *Physical Review A* **85**, 022322 (2012), 1006.4368.
- [44] P. Hauke, M. Heyl, L. Tagliacozzo, and P. Zoller, Measuring multipartite entanglement via dynamic susceptibilities, *Nature Physics* **12**, 778 (2016), 1509.01739.
- [45] T. Grover and M. P. A. Fisher, Quantum disentangled liquids, *Journal of Statistical Mechanics: Theory and Experiment* **2014**, P10010 (2014), 1307.2288.
- [46] D. Ben-Zion, J. McGreevy, and T. Grover, Disentangling quantum matter with measurements, *Physical Review B* **101**, 115131 (2020), 1912.01027.
- [47] A. Smith, J. Knolle, R. Moessner, and D. L. Kovrizhin, Absence of ergodicity without quenched disorder: from quantum disentangled liquids to many-body localization, *Physical Review Letters* **119**, 176601 (2017), 1705.09143.
- [48] G. Vidal, J. I. Latorre, E. Rico, and A. Kitaev, Entanglement in quantum critical phenomena, *Physical Review Letters* **90**, 227902 (2003), quant-ph/0211074v1.
- [49] I. Peschel, Calculation of reduced density matrices from correlation functions, *Journal of Physics A: Mathematical and General* **36**, L205 (2003), cond-mat/0212631v1.
- [50] O. Hart, S. Gopalakrishnan, and C. Castelnovo, Logarithmic entanglement growth from disorder-free localization in the two-leg compass ladder, *Phys. Rev. Lett.* **126**, 227202 (2021).
- [51] M. Serbyn, Z. Papić, and D. A. Abanin, Universal slow growth of entanglement in interacting strongly disordered systems, *Physical Review Letters* **110**, 260601 (2013), 1304.4605.
- [52] A. Polkovnikov, Microscopic diagonal entropy and its connection to basic thermodynamic relations, *Annals of Physics* **326**, 486 (2011), 0806.2862.
- [53] H.-H. Lai and K. Yang, Entanglement entropy scaling laws and eigenstate typicality in free fermion systems, *Physical Review B* **91**, 081110 (2015), 1409.1224.
- [54] C. H. Lee, P. Ye, and X.-L. Qi, Position momentum duality in the entanglement spectrum of free fermions, *Journal of Statistical Mechanics: Theory and Experiment* **2014**, P10023 (2014), 1403.1039.
- [55] H. K. Janssen, B. Schaub, and B. Schmittmann, New universal short-time scaling behaviour of critical relaxation processes, *Zeitschrift für Physik B Condensed Matter* **73**, 539 (1989).
- [56] V. Oganesyan and D. A. Huse, Localization of interacting fermions at high temperature, *Physical Review B* **75**, 155111 (2007), cond-mat/0610854v1.
- [57] T. Devakul and D. A. Huse, Anderson localization transitions with and without random potentials, *Physical Review B* **96**, 214201 (2017), 1709.01521.
- [58] A. MacKinnon and B. Kramer, One-parameter scaling of localization length and conductance in disordered systems, *Physical Review Letters* **47**, 1546 (1981).
- [59] A. MacKinnon and B. Kramer, The scaling theory of electrons in disordered solids: Additional numerical results, *Zeitschrift für Physik B Condensed Matter* **53**, 1 (1983).
- [60] P. Markos, Numerical analysis of the anderson localization, *Acta Physica Slovaca. Reviews and Tutorials* **56**, 10.2478/v10155-010-0081-0 (2006), cond-mat/0609580v1.
- [61] J. Bellissard, A. van Elst, and H. S. Baldes, The non-commutative geometry of the quantum hall effect, *Journal of Mathematical Physics* **35**, 5373 (1994).
- [62] E. Prodan, T. L. Hughes, and B. A. Bernevig, Entanglement spectrum of a disordered topological chern insula-

- tor, *Physical Review Letters* **105**, 115501, 1005.5148v2.
- [63] R. Bianco and R. Resta, Mapping topological order in coordinate space, *Physical Review B* **84**, 241106 (2011), 1111.5697v3.
- [64] N. Read and D. Green, Paired states of fermions in two dimensions with breaking of parity and time-reversal symmetries, and the fractional quantum hall effect, *Physical Review B* **61**, 10267 (2000), cond-mat/9906453v3.
- [65] T. Senthil and M. P. A. Fisher, Quasiparticle localization in superconductors with spin-orbit scattering, *Physical Review B* **61**, 9690 (2000), cond-mat/9906290v1.
- [66] J. T. Chalker, N. Read, V. Kagalovsky, B. Horovitz, Y. Avishai, and A. W. W. Ludwig, Thermal metal in network models of a disordered two-dimensional superconductor, *Physical Review B* **65**, 012506 (2001), cond-mat/0009463v1.
- [67] C. R. Laumann, A. W. W. Ludwig, D. A. Huse, and S. Trebst, Disorder-induced majorana metal in interacting non-abelian anyon systems, *Physical Review B* **85**, 161301 (2012), 1106.6265v2.
- [68] V. Lahtinen, A. W. W. Ludwig, J. K. Pachos, and S. Trebst, Topological liquid nucleation induced by vortex-vortex interactions in kitaev's honeycomb model, *Physical Review B* **86**, 075115 (2012), 1111.3296v4.
- [69] C. N. Self, J. Knolle, S. Iblisdir, and J. K. Pachos, Thermally induced metallic phase in a gapped quantum spin liquid - a monte carlo study of the kitaev model with parity projection, *Physical Review B* **99**, 045142 (2019), 1807.07926v2.
- [70] A. Weisse, G. Wellein, A. Alvermann, and H. Fehske, The kernel polynomial method, *Reviews of Modern Physics* **78**, 275 (2006), cond-mat/0504627v2.
- [71] C. Wang, A. Vishwanath, and B. I. Halperin, Topological order from disorder and the quantized hall thermal metal: Possible applications to the $\nu = 5/2$ state, *Physical Review B* **98**, 045112 (2018), 1711.11557v3.
- [72] D. J. Thouless, M. Kohmoto, M. P. Nightingale, and M. den Nijs, Quantized hall conductance in a two-dimensional periodic potential, *Phys. Rev. Lett.* **49**, 405 (1982).
- [73] Q. Niu, D. J. Thouless, and Y.-S. Wu, Quantized hall conductance as a topological invariant, *Phys. Rev. B* **31**, 3372 (1985).
- [74] T. Fukui, Y. Hatsugai, and H. Suzuki, Chern numbers in discretized brillouin zone: Efficient method of computing (spin) hall conductances, *Journal of the Physical Society of Japan* **74**, 1674 (2005), cond-mat/0503172v2.
- [75] D. P. Arovas, R. N. Bhatt, F. D. M. Haldane, P. B. Littlewood, and R. Rammal, Localization, wave-function topology, and the integer quantized hall effect, *Physical Review Letters* **60**, 619 (1988).
- [76] F. Evers and A. D. Mirlin, Anderson transitions, *Reviews of Modern Physics* **80**, 1355 (2008), 0707.4378v1.
- [77] B. I. Halperin, Quantized hall conductance, current-carrying edge states, and the existence of extended states in a two-dimensional disordered potential, *Phys. Rev. B* **25**, 2185 (1982).
- [78] Y. Huo and R. N. Bhatt, Current carrying states in the lowest landau level, *Physical Review Letters* **68**, 1375 (1992).
- [79] A. C. Potter and R. Vasseur, Symmetry constraints on many-body localization, *Physical Review B* **94**, 224206 (2016), 1605.03601.
- [80] G. D. Tomasi, F. Pollmann, and M. Heyl, Solving efficiently the dynamics of many-body localized systems at strong disorder, *Physical Review B* **99**, 241114 (2019), 1810.04178v2.
- [81] L. M. Robledo, The sign of the overlap of hfb wave functions, *Physical Review C* **79**, 021302 (2009), 0901.3213.
- [82] M. Fagotti and P. Calabrese, Entanglement entropy of two disjoint blocks in XY chains, *Journal of Statistical Mechanics: Theory and Experiment* **2010**, P04016 (2010).
- [83] M. Wimmer, Efficient numerical computation of the pfaffian for dense and banded skew-symmetric matrices, *ACM Transactions on Mathematical Software* **38**, 1 (2012), 1102.3440.
- [84] I. Klich, Full counting statistics: An elementary derivation of levitov's formula, cond-mat/0209642v1.
- [85] I. Klich, A note on the full counting statistics of paired fermions, *Journal of Statistical Mechanics: Theory and Experiment* **2014**, P11006 (2014), 1403.7824v2.
- [86] I. L. Aleiner, B. L. Altshuler, and G. V. Shlyapnikov, Finite temperature phase transition for disordered weakly interacting bosons in one dimension, *Nature Physics* **6**, 900 (2010), 0910.4534.
- [87] C. Nayak, S. H. Simon, A. Stern, M. Freedman, and S. D. Sarma, Non-abelian anyons and topological quantum computation, *Reviews of Modern Physics* **80**, 1083 (2008), 0707.1889.
- [88] A. Y. Kitaev, Fault-tolerant quantum computation by anyons, *Annals of Physics* **303**, 2 (2003), quant-ph/9707021.
- [89] C. de C. Chamon, C. Mudry, and X.-G. Wen, Gaussian field theories, random cantor sets and multifractality, *Physical Review Letters* **77**, 4194 (1996), cond-mat/9510088.
- [90] Y. Hatsugai, X.-G. Wen, and M. Kohmoto, Disordered critical wave functions in random bond models in two dimensions - random lattice fermions at $e = 0$ without doubling, *Physical Review B* **56**, 1061 (1997), cond-mat/9603169.
- [91] A. Altland and B. D. Simons, Field theory of the random flux model, *Journal of Physics A: Mathematical and General* **32**, L353 (1999), cond-mat/9811134.
- [92] O. Hart, Y. Wan, and C. Castelnovo, Coherent propagation of quasiparticles in topological spin liquids at finite temperature, *Physical Review B* **101**, 064428 (2020), 1909.08633v2.
- [93] A. Russomanno, S. Notarnicola, F. M. Surace, R. Fazio, M. Dalmonte, and M. Heyl, Homogeneous floquet time crystal protected by gauge invariance, *Physical Review Research* **2**, 012003 (2020), 1906.03185v2.
- [94] H. C. Po, L. Fidkowski, A. Vishwanath, and A. C. Potter, Radical chiral floquet phases in a periodically driven kitaev model and beyond, *Physical Review B* **96**, 245116 (2017), 1701.01440.
- [95] I. C. Fulga, M. Maksymenko, M. T. Rieder, N. H. Lindner, and E. Berg, Topology and localization of a periodically driven kitaev model, *Physical Review B* **99**, 235408 (2019), 1902.06995.
- [96] L.-M. Duan, E. Demler, and M. D. Lukin, Controlling spin exchange interactions of ultracold atoms in optical lattices, *Phys. Rev. Lett.* **91**, 090402 (2003).
- [97] A. Micheli, G. Brennen, and P. Zoller, A toolbox for lattice-spin models with polar molecules, *Nature*

- Physics **2**, 341 (2006).
- [98] J. Q. You, X.-F. Shi, X. Hu, and F. Nori, Quantum emulation of a spin system with topologically protected ground states using superconducting quantum circuits, *Phys. Rev. B* **81**, 014505 (2010).
- [99] M. Sameti and M. J. Hartmann, Floquet engineering in superconducting circuits: From arbitrary spin-spin interactions to the kitaev honeycomb model, *Phys. Rev. A* **99**, 012333 (2019).
- [100] G. Kells, V. Lahtinen, and J. Vala, Kitaev spin models from topological nanowire networks, *Phys. Rev. B* **89**, 075122 (2014).
- [101] E. Sagi, H. Ebisu, Y. Tanaka, A. Stern, and Y. Oreg, Spin liquids from majorana zero modes in a cooper-pair box, *Phys. Rev. B* **99**, 075107 (2019).
- [102] H. Zhang, S. Kim, Y.-J. Kim, H.-Y. Kee, and L. Yang, Ultrafast dynamics of fractional particles in α -RuCl₃, *arXiv e-prints*, arXiv:1908.04807 (2019), arXiv:1908.04807 [cond-mat.str-el].
- [103] J. Knolle and R. Moessner, A field guide to spin liquids, *Annual Review of Condensed Matter Physics* **10**, 451 (2019), <https://doi.org/10.1146/annurev-conmatphys-031218-013401>.
- [104] Y. Motome and J. Nasu, Hunting majorana fermions in kitaev magnets, *Journal of the Physical Society of Japan* **89**, 012002 (2020), <https://doi.org/10.7566/JPSJ.89.012002>.
- [105] M. Ye, R. M. Fernandes, and N. B. Perkins, Phonon dynamics in the kitaev spin liquid, *Phys. Rev. Research* **2**, 033180 (2020).
- [106] A. Metavitsiadis and W. Brenig, Phonon renormalization in the kitaev quantum spin liquid, *Phys. Rev. B* **101**, 035103 (2020).
-

Appendix A: Tuning density of random π fluxes

The quantum quench protocol with a prequench spin product state excites all the allowed gauge configurations like in a thermal ensemble of infinite temperature, where the typical gauge configuration is maximally random. It is also interesting to see the dynamics interpolating between the clean limit and this dirty limit, analogous to tuning the temperature from zero to infinite in a thermal ensemble. In general there could be three related but inequivalent ways of interpolating between the zero gauge flux configuration and the typical maximally random gauge flux configuration. The first way is to endow any specific gauge field configuration with a thermal weight depending on the corresponding Majorana fermion free energy, which is commonly used in Monte Carlo calculations for finite temperature thermal ensemble [23]. The second way is simply to tune the density of π link: $p(u = -1) \in [0, 0.5]$ [67]. But notice that the gauge field on a link is not gauge invariant quantity. The third interpolation way is to tune the average gauge-invariant flux [24] by applying the spin ring exchange interaction operator $\prod_q (1/2 + (1/2 - p)\hat{W})$ to the initial state, which is equivalent to tuning the density of π flux on a hexagon plaquette from 0 to 0.5. One could even further extend this range to $p \in [0, 1]$ to interpolate between the absolute 0 flux and fully packed π flux gauge configurations [68], with the dirty limit lying in between. This manner of controlling the density of π flux can be realized by deforming the quench protocol and hence the initial state $|\Psi_0(p)\rangle$, where the fermion maintains in a gauged vacuum in each gauge configuration $\langle \Psi_0(p) | iu\alpha\beta | \Psi_0(p) \rangle = 1$.

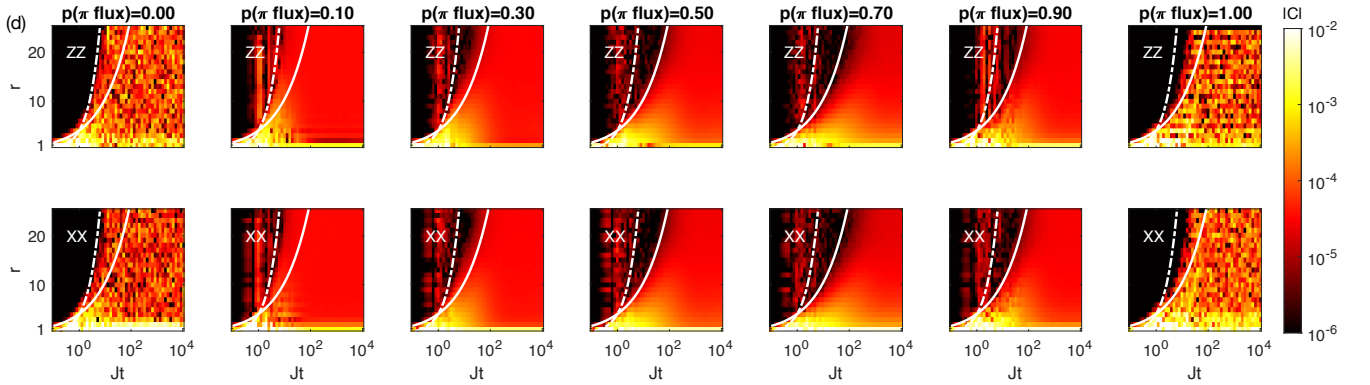


FIG. 7. Correlation light cones by tuning the density of π fluxes. Upper(bottom) panel is for $C^{zz(xx)}$. To guide the eyes, white solid line shows subdiffusive propagation $r = 4(Jt)^{1/2.4}$ expected for $p = 0.5$, while white dot dashed line indicates ballistic propagation $r = 4Jt$. Each column stands for a given density of π flux. Parameters: $J_z = J_x = J_y \equiv J, \tilde{h} = 0.25J, L_x = L_y = 50$, 1000 disorder samples.

As shown in Fig. 7a, at intermediate time, the projected Majorana bipartite entanglement entropy grows algebraically with non-monotonically varying exponent depending on the density of random π fluxes. In Fig. 7bc, the late time steady state exhibits algebraic dimer correlation functions in space, with a non-monotonically continuously varying exponent. Overall, the cleaner system with p close to 0 or 1 have faster information propagation, but less prominent critical correlation in steady state. Notice that the maximally random case $p = 0.5$ does not yield the slowest entanglement propagation nor the largest correlation exponent, which might be due to the asymmetry between the clean 0 flux sector and π flux sector. From this discrete sequence of disorder density, we do not find divergent tendency for the dynamical exponent like in the MBL phase transition, which is consistent with the fact that non-Abelian topological phases of matter cannot be fully localized [79]. In Fig. 7d, we show the spatiotemporal profiles of the dimer quantum correlation functions, where a continuously varying light-cone is witnessed. The clean limit without disorder exhibits oscillation inside the lightcone due to the finite size non-interacting nature, which is damped by the onset of disorder.

Appendix B: Other Majorana fermion correlations

Throughout the main text we mainly consider the physical observable of spin dimers, which is equivalent to the next nearest neighbouring gauge invariant Majorana fermion bilinear term. This is the simplest and most natural choice in both spin and fermion representation. However, the spin dimer correlation might be much more difficult to measure in experiments than the spin correlation. The single bare spin operator is composed of single matter Majorana fermion and an auxiliary Majorana operator that flips the gauge connection and subsequently the fluxes. Nevertheless, it was

shown in Ref. [22] that the flux-conservation-breaking perturbation could generally dress the spin operator and lead to a contribution of pure matter Majorana fermion bilinear term that preserves the flux. For example, to leading order $\tilde{\sigma}^z \approx \sigma^z + f\sigma^x\sigma^z\sigma^y + \dots$, where the second term is just the three-spin interaction in an neighbouring wedge, transformed to the next nearest neighbour hopping term of the Majorana fermions on the same sublattice. In low energy, this term contributes to the chiral mass of the Majorana fermion. This pure matter contribution qualitatively changes the low temperature low frequency spin spin correlation function [22]. Here we also perform a modest calculation for the spreading of (i) correlation between two Majorana fermions on the same sublattice, separated at a distance; (ii) connected correlation between two next-nearest-neighbour-Majorana-fermion-bilinears on the same sublattice. The latter one should contribute to the spin spin correlation that is accessible by experimental probe. As shown in Fig. 8, the spread of this correlation appears to be consistent with the subdiffusive fermion entanglement growth we show in the main-text. In the late time steady state, the correlations also appears to show a power-law signature. Therefore, the subdiffusive dynamics and critical correlation we obtain may leave signatures in the pump-probe experiments for transient spin dynamics.

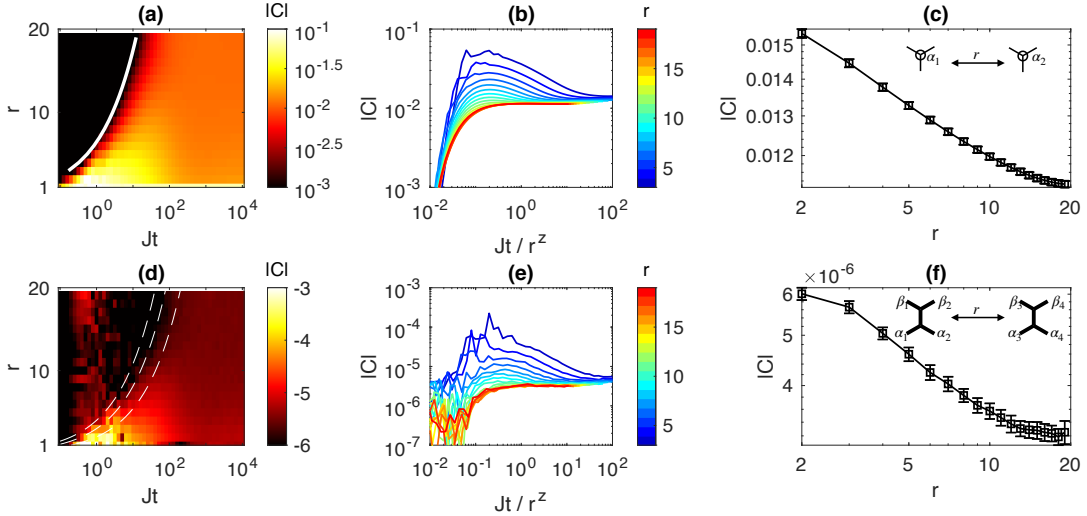


FIG. 8. Spreading of Majorana fermion correlation function (upper panel) and Majorana bilinear correlation function (bottom panel) on the same sublattice. (a) Spatiotemporal tomography of the spreading of Majorana fermion correlation, $|\langle \alpha_j(t) \alpha_{j+r}(t) \rangle|$, being averaged over sites and sublattices and random gauge configurations. By taking a threshold $|C| > 10^6$, we fit the propagating front $r \propto t^{1/z}$ where $z = 2.3(2)$. (b) Collapse of the growth of correlation function in a rescaled time Jt/r^z . (c) Correlation function in steady state, averaged over time window $10^3 < Jt < 10^4$. Inset shows schematically the fermionic two-point correlation function. (d) Spatiotemporal tomography of the spreading of next-nearest-neighbour-Majorana-bilinear correlation function, $\frac{1}{2^N} \sum_{\{u\}} \langle \psi_u(t) | i\alpha_1 \alpha_2 i\alpha_3 \alpha_4 | \psi_u(t) \rangle - \left(\frac{1}{2^N} \sum_{\{u\}} \langle \psi_u(t) | i\alpha_1 \alpha_2 | \psi_u(t) \rangle \right)^2$, averaged over the sublattices. Despite the large disorder sample size, the statistical fluctuation in small time is still relatively strong compared to the saturated values. Dashed lines show $r = 2t^{1/z}$, $r = 3t^{1/z}$, $r = 4t^{1/z}$ respectively to guide the eyes for the propagating wave-front. (e) Collapse of the growth of correlation function in a rescaled time Jt/r^z . (f) Correlation function in steady state, averaged over time window $10^3 < Jt < 10^4$. Inset shows schematically the correlation function. Parameters: $J_z = J_x = J_y \equiv J$, $\hbar = 0.25J$, $L_x = L_y = 40$, 10000 disorder samples.

Appendix C: Anisotropic coupling: beyond low energy universality class

It is tempting to ask whether the critical dynamical phase we obtain out of a nonequilibrium quantum quench is associated with the low energy topological phases. To answer this question we may tune the Kitaev interaction to be strongly anisotropic, by choosing $J_z = 2J$, $J_x = J_y = 0.5J$, $\hbar = 0.25J$. In this case at zero temperature it belongs to the Abelian \mathbb{Z}_2 topological phase, in the same universality class with the celebrated toric code model. In fact, the low energy physics of the anisotropic Kitaev honeycomb model can be mapped to the toric code model [20]. However, at high energy density the connection between the Kitaev honeycomb model and the toric code model is not *a priori* known.

The perturbed toric code model was argued to be many-body localized in the presence of strong disorder [41], since it can be dual to the Ising model when charge is absent [88]. The anisotropic Kitaev honeycomb model in the presence of magnetic field, on the other hand, is found to exhibit subdiffusive spreading of quantum correlation and

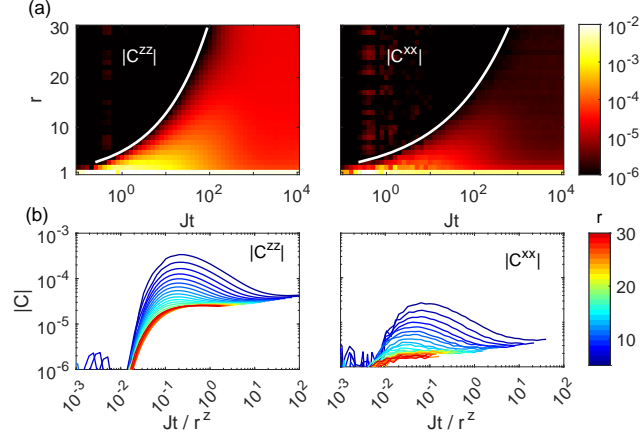


FIG. 9. Anisotropic coupling $J_z = 2J, J_x = J_y = 0.5J, \tilde{h} = 0.25J$. (a) Anisotropic algebraic lightcone of dimer correlation spreading. $L_x = L_y = 60$, 1000 disorder samples. White line shows the fitted wave-front using the same threshold as in main text which follows $r \propto (Jt)^{1/z'}$, where $z' = 2.6(2)$ for C^{zz} and $z' = 3.4(2)$ for C^{xx} . (b) Dimer correlation at fixed distances versus rescaled time using z' fitted from entanglement entropy growth below.

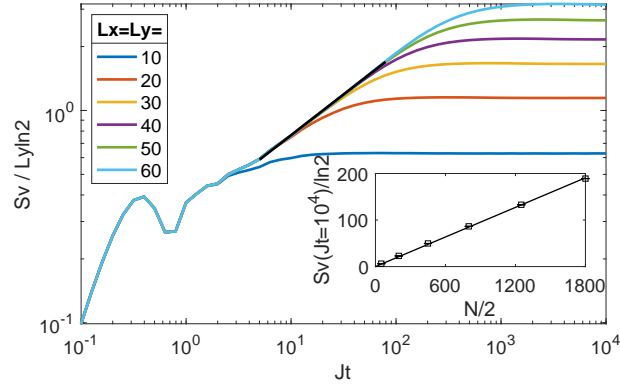


FIG. 10. Anisotropic coupling $J_z = 2J, J_x = J_y = 0.5J, \tilde{h} = 0.25J$. Projective entanglement entropy. Black line is for power-law fit $\propto (Jt)^{1/z'}$ where $z' = 2.6(1)$, consistent with the spreading of C^{zz} .

entanglement, see Fig. 9 and Fig. 10. Notice that the spreading of dimer correlation is anisotropic, and that along z direction has the same exponent as the spreading of entanglement. Behind that we also find the topological critical fermion modes at high energy for the random flux configurations or π -flux configuration, even though the zero energy ground state is topological trivial, see Fig. 11. It means that unlike the 0 flux sector, the random flux sectors cannot be adiabatically connected to the toric code limit without closing the mobility gap at certain energy. The late-time steady state also exhibits critical dimer correlation along z -direction, see Fig. 12. These evidences show that the critical dynamics phase goes beyond the low energy effective theory. The topological critical Majorana modes at high energy are responsible for the anomalous subdiffusive dynamics and critical correlation.

Appendix D: Dynamics in the absence of magnetic field

For completeness, we also compute the dynamics for the time reversal symmetric Kitaev model in the absence of magnetic field $h = 0$, as shown in Fig. 13. In such case, the problem is equivalent to a free Majorana fermion with only nearest neighbour hopping on the honeycomb lattice, that is exposed to a random π flux penetrating the plaquette. Notice that without magnetic field there is not only time reversal symmetry but also the sublattice (chiral) symmetry (sign change to one sublattice changes the sign of the Hamiltonian), which connects the positive energy to negative energy but acts as a unitary symmetry distinct from the anti-unitary particle hole symmetry. The zero energy single particle mode has exact chiral symmetry, and therefore often behaves qualitatively distinct from the other energy

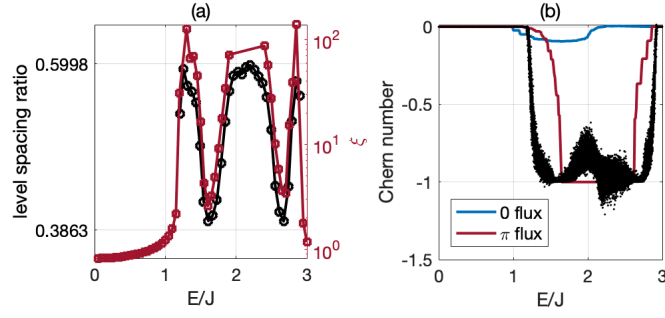


FIG. 11. Anisotropic coupling $J_z = 2J, J_x = J_y = 0.5J, \tilde{h} = 0.25J$. Localization analysis by (a) level spacing ratio and localization length, and (b) Chern number.

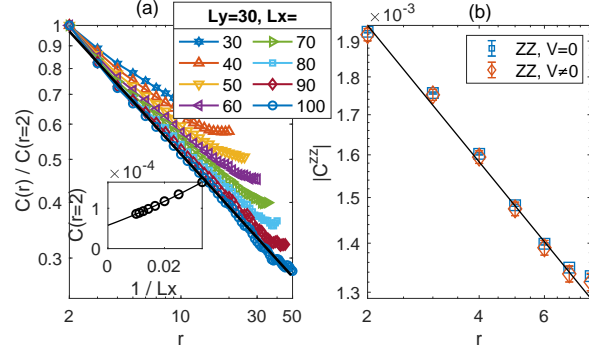


FIG. 12. Anisotropic coupling $J_z = 2J, J_x = J_y = 0.5J, \tilde{h} = 0.25J$. (a) Non-interacting steady state correlation C^{zz} for large system sizes. The black line indicates the fitted power-law behaviour $\propto r^{-\Delta'}$ where $\Delta' = 0.39(1)$. (b) Interacting steady state correlation C^{zz} , with the non-interacting case in comparison, for system size 16×4 . Fitted power-law $\propto r^{-\Delta''}$ where $\Delta'' = 0.30(4)$.

states in the presence of disorder. A closely related problem is the gapless Dirac fermion in the presence of random $U(1)$ magnetic flux disorder, see Ref. [89–91]. Here we are dealing with a Majorana version of the Dirac fermion in the presence of π flux disorder, with additional particle hole symmetry. As shown in Fig. 14, our numerical result suggests a diverging localization length towards zero energy. Besides, there seems to be multiple singular points.

For comparison, we summarize the dynamical exponents fit from different physical observables and for different parameter regime as in Table. I.

J_z/J	J_x/J	J_y/J	\tilde{h}	z_{zz}	z_{xx}	z_{ent}
1.0	1.0	1.0	0.25	2.5(2)	2.7(3)	2.4(1)
2.0	0.5	0.5	0.25	2.6(2)	3.4(2)	2.6(1)
1.0	1.0	1.0	0.00	2.0(5)	1.7(3)	2.1(2)

TABLE I. Fit dynamical exponent.

Appendix E: Fermionization for Hamiltonian and state

Below we review two alternative fermionization approaches for the Kitaev model, and draw the connections between them. Generally speaking, Kitaev’s original gauge theory approach is physically transparent and looks more symmetric in putting gauge field on every link, while the Jordan Wigner transformation approach [35] is practically convenient without gauge redundancy. The latter can be achieved from the former by gauge fixing, with proper care taken for the boundary terms.

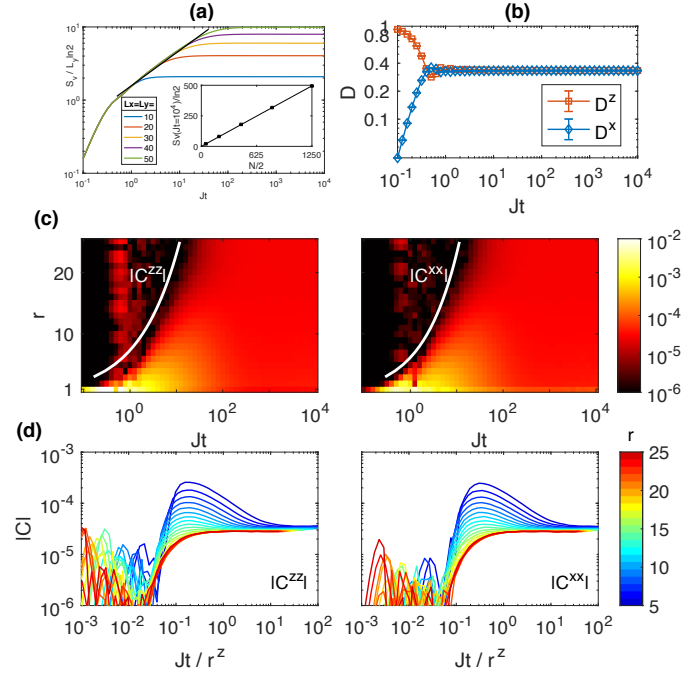


FIG. 13. Numerical results for the gapless Kitaev model without magnetic field $J_z = J_x = J_y = J, h = 0$. (a) Projective bipartite entanglement entropy. Black line is for power-law fit $\propto (Jt)^{1/z}$ where $z = 2.1(2)$. (b) Dimer expectations. (c) Algebraic lightcone of dimer correlation spreading. $L_x = L_y = 50$, 1000 disorder samples. White line shows $r \propto (Jt)^{1/z}$ where $z = 2.0(5)$ for C^{zz} and $z = 1.7(3)$ for C^{xx} . (d) Dimer correlation at fixed distances versus rescaled time using z fitted from the corresponding correlation function.

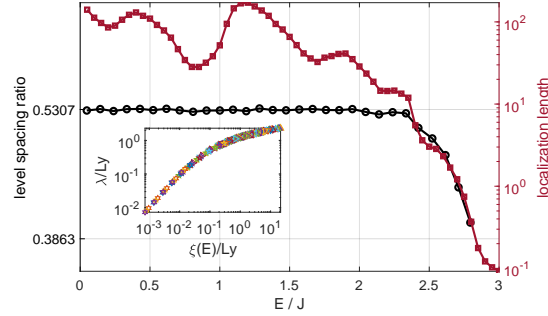


FIG. 14. Localization analysis for the time reversal symmetric Kitaev model without magnetic field $J_x = J_y = J_z = J, h = 0$, which is mapped to a free Majorana fermion hopping on a honeycomb lattice with random π flux disorder. Left axis: level spacing ratio calculated from 1000 disorder samples of system size $L_x = L_y = 50$, where the Poisson value $2 \ln 2 - 1 \approx 0.3863$ and the Gaussian orthogonal ensemble value ≈ 0.5307 are indicated. Right axis: localization length calculated in quasi-1D stripes with $L_y = 8, 16, 32, 64, 128$ while $L_x \leq 10^6$. The recursive iteration for Green's function is stopped when relative deviation of the smallest Lyapunov exponent gets smaller than 0.1 or $L_x = 10^6$. Inset shows the data collapse of the one parameter scaling ansatz, for different stripe widths and energies.

1. Jordan-Wigner transformation

As a warmup let us first consider only one zig-zag row composed of x -links and y -links: $\sum_{j \in A} \sigma_j^x \sigma_{j+1}^x + \sum_{j \in B} \sigma_j^y \sigma_{j+1}^y$. It can be readily solved by performing a zigzag Jordan-Wigner transformation:

$$\sigma_{j \in A}^x = \left(\prod_{i=1}^{j-1} \sigma_i^z \right) b_j, \quad \sigma_{j \in A}^y = + \left(\prod_{i=1}^{j-1} \sigma_i^z \right) \alpha_j, \quad \sigma_{j \in A}^z = -i b_j \alpha_j, \quad \sigma_{j \in B}^x = \left(\prod_{i=1}^{j-1} \sigma_i^z \right) \beta_j, \quad \sigma_{j \in B}^y = - \left(\prod_{i=1}^{j-1} \sigma_i^z \right) b_j, \quad \sigma_{j \in B}^z = i \beta_j b_j, \quad (\text{E1})$$

such that the Ising exchange interactions on $x(y)$ -links are simplified to Majorana fermion hopping terms

$$\sigma_{j \in A}^x \sigma_{j+1}^x = -i\alpha_j \beta_{j+1}, \quad \sigma_{j \in B}^y \sigma_{j+1}^y = -i\alpha_{j+1} \beta_j. \quad (\text{E2})$$

Now consider the honeycomb lattice, where spins are ordered row by row to be Jordan-Wigner transformed, and we label the sites by row and column indices (i, j) . The above intra-row interactions remain unchanged, while the inter-row couplings are simply

$$\sigma_{i,j \in A}^z \sigma_{i+1,j}^z = -i\alpha_{i,j} \beta_{i+1,j} (i b_{i,j} b_{i+1,j}) \equiv -i\alpha_{i,j} \beta_{i+1,j} u_{i,j}^z, \quad (\text{E3})$$

where a static link variable $u_{i,j}^z = \pm 1$ emerges on every z -link. Therefore the three anisotropic Ising interactions become free Majorana hopping terms coupled with classical \mathbb{Z}_2 variables. Since Jordan-Wigner transform is a non-local unitary, the boundary term in each row yields a non-local term:

$$\sigma_{i,2L_x}^y \sigma_{i,1}^y = -i\alpha_{i,1} \beta_{i,2L_x} \left(-\prod_{k=1}^{2L_x} \sigma_{i,k}^z \right) \equiv i\alpha_{i,1} \beta_{i,2L_x} u_i^y, \quad (\text{E4})$$

where u_i^y commutes with the Hamiltonian therefore serves as a conserved quantum number, separating the fermion system into disconnected sectors with distinct boundary condition. In other words, the spin model with a definite boundary condition contain two fermion sectors with distinct boundary condition for fermions, which is reminiscent of the 1D quantum Ising critical point.

Here we briefly comment that the boundary condition in fermion basis is relevant to the topological ground state degeneracy, which is generated by moving two \mathbb{Z}_2 local gauge fluxes around the torus before annihilation, equivalent to pumping a global \mathbb{Z}_2 flux for fermions [87]. In the Abelian phase (toric code), one obtains 4-fold degeneracy by the freedom of pumping global \mathbb{Z}_2 flux along either direction. In the non-Abelian Ising phase, there are only 3-fold degeneracy, because due to the Majorana zero mode trapped by the flux, pumping global flux along both directions would leave a global fermionic excitation behind and take the state away from ground state manifold.

Under such Jordan Wigner transformation, the prequench initial spin polarized product state that satisfies

$$\sigma_{j \in A}^z |\Psi_0\rangle = -i b_{j \in A} \alpha_j |\Psi_0\rangle = -|\Psi_0\rangle, \quad \sigma_{j \in B}^z |\Psi_0\rangle = i \beta_j b_{j \in B} |\Psi_0\rangle = |\Psi_0\rangle, \quad (\text{E5})$$

is transformed to a product state of local Majorana dimers satisfying $i b_{j \in A} \alpha_j = 1$, $i \beta_j b_{j \in B} = 1$. By grouping (b, b) and (α, β) , it is a maximally entangled EPR state between the local Majorana bilinears and the gauge field on z -link:

$$|\Psi_0\rangle = \prod_j \frac{1}{\sqrt{2}} (|i\alpha_j \beta_{j-e_z} = 1\rangle |u_j = 1\rangle + |i\alpha_j \beta_j = -1\rangle |u_j = -1\rangle). \quad (\text{E6})$$

Therefore the prequench state is a gauged fermion vacuum state with disordered gauge configurations. The post-quench Hamiltonian can be viewed as a Bogoliubov-de-Gennes superconducting Hamiltonian with gauged pairing and hopping terms, which would create fermion pairs from the gauged vacuum and allow them to propagate. On the other hand, such initial state projects onto the sector that locks opposite boundary condition between spin and fermion representations i.e. $-\sigma^y \sigma^y = -i\alpha\beta$ on boundary while $\sigma^y \sigma^y = -i\alpha\beta$ in the bulk. We'll work with the anti-periodic boundary condition for the spin model, and hence periodic boundary condition for the Majorana fermions.

2. Redundant gauge theory

Kitaev's original solution [20] is to extend the Hilbert space by rewriting each spin operator by four Majorana fermions with a physical constraint:

$$\sigma_j^{x(y)(z)} = i b_j^{x(y)(z)} c_j, \quad -i \sigma_j^x \sigma_j^y \sigma_j^z = 1 = b_j^x b_j^y b_j^z c_j. \quad (\text{E7})$$

Then the spin Hamiltonian rewritten in terms of Majorana fermions are always trivially conserved by $e^{i\pi G} \equiv b_j^x b_j^y b_j^z c_j$. In other words, the subsequent Hamiltonian in terms of Majorana fermions by definition has a \mathbb{Z}_2 gauge symmetry, generated by $e^{i\pi G}$. Notice that G is the \mathbb{Z}_2 analogue of the Gauss law operator $n_j - \sum_k E_{j,k}$ as in the conventional U(1) gauge theory. The constraint $b_j^x b_j^y b_j^z c_j = 1$ actually picks up the gauge neutral sector among all other super-selection sectors to be the physical space, as a superposition of all gauge equivalent configurations.

In the exact solvable regime, the \mathbb{Z}_2 gauge field on every link $u_j^{x(y)(z)} \equiv i b_j^{x(y)(z)} b_{j-e_{x(y)(z)}}^{x(y)(z)}$ is conserved. To avoid extensive redundancy, one can always use the gauge transformation to fix the gauge such that $u_j^{x(y)} = 1$ on every

link in the bulk. In other words, the gauge field is oriented only towards z-direction, analogous to the Landau gauge. However, one should pay special attention when the lattice is not on a planar but a compact manifold such as torus. In a torus, there could be global fluxes which can neither be detected locally nor be locally gauged away. Therefore, there must remain $u_j^{x(y)} \neq 1$ on certain boundary links that account for the global fluxes. One can also see this by taking the product of gauge neutral constraints along one zig-zag row: $\prod_{j \in \text{row}} u_j^x u_j^y = -\prod_{j \in \text{row}} \sigma_j^z$. Therefore one may fix $u_j^{x(y)} = 1$ in the bulk but must allow one boundary x(y)-link on every row fluctuating, which is equal to $-\prod_{j \in \text{row}} \sigma_j^z$. In this way, we reach exactly the same fermionic Hamiltonian with a nonlocal boundary term, as derived from Jordan-Wigner transformation. And in this way we shall see that the \mathbb{Z}_2 variable emergent in Jordan Wigner transformation has the physical meaning of a gauge field.

Last but not least, one should notice that the onset of magnetic field does not explicitly spoils the \mathbb{Z}_2 gauge symmetry of fermion since that is just a gauge redundancy in the extended Hilbert space. Instead, the magnetic field breaks another set of local \mathbb{Z}_2 symmetries which stand for the gauge flux conservation.

Appendix F: Observables at exact solvable regime

For convenience let us label the unitcell(z-link) by j in the following and group the Majorana fermions into a $2N$ -dimensional vector $\zeta \equiv \begin{pmatrix} \alpha \\ \beta \end{pmatrix}$, such that $\zeta_{j=1, \dots, N}$ specifies α , and $\zeta_{j=N+1, \dots, 2N}$ specifies β . The Gaussian evolution operator acting on the free Majorana fermion reduces to an $2N$ -by- $2N$ evolution matrix $\zeta(t) = e^{[it\hat{H}]} \zeta = e^{-i2tH} \zeta$. Therefore one can keep track of the time evolved two-Majorana-fermion covariant matrix:

$$\Gamma(t) \equiv \frac{i}{2} \langle [\zeta(t), \zeta^T(t)] \rangle = e^{-i2tH} i\tau^y \otimes (\oplus_j u_j) e^{i2tH}, \quad (\text{F1})$$

which is skew-symmetric matrix. The matrix elements immediately give the spin dimer expectations expressed in terms of gauged Majorana fermion bilinears:

$$\langle D_j^z(t) \rangle = \langle iu_j \alpha_j(t) \beta_j(t) \rangle = u_j \Gamma(t)_{j, j+N}, \quad \langle D_j^x(t) \rangle = \langle i\alpha_j(t) \beta_{j+n_2}(t) \rangle = \Gamma(t)_{j, j+n_2+N}. \quad (\text{F2})$$

The disconnected dimer correlation functions expressed in terms of the four-Majorana-fermion correlation functions can be decomposed using Wick's theorem

$$\begin{aligned} C_j^{zz}(r, t) &\equiv \langle D_j^z(t) D_{j+r}^z(t) \rangle = u_j u_{j+r} \langle i\alpha_j(t) \beta_j(t) i\alpha_{j+r n_1}(t) \beta_{j+r n_1}(t) \rangle \\ &= u_j u_{j+r n_1} \{ \langle i\alpha_j(t) \beta_j(t) \rangle \langle i\alpha_{j+r n_1}(t) \beta_{j+r n_1}(t) \rangle - \langle i\alpha_j(t) \alpha_{j+r n_1}(t) \rangle \langle i\beta_j(t) \beta_{j+r n_1}(t) \rangle - \langle i\alpha_j(t) \beta_{j+r n_1}(t) \rangle \langle i\alpha_{j+r n_1}(t) \beta_j(t) \rangle \} \\ &= u_j u_{j+r n_1} (\Gamma(t)_{j, j+N} \Gamma(t)_{j+r n_1, j+r n_1+N} - \Gamma(t)_{j, j+r n_1} \Gamma(t)_{j+N, j+r n_1+N} - \Gamma(t)_{j, j+r n_1+N} \Gamma(t)_{j+r n_1, j+N}). \end{aligned} \quad (\text{F3})$$

Likewise for C^{xx} .

In each gauge configuration, the time evolved density operator is Gaussian. Therefore the reduced density operator of the half-partitioned fermion system is also a Gaussian density operator that can be disentangled into reduced canonical fermions denoted as d_n , $n = 1, \dots, N/2$:

$$\hat{\rho}_r \equiv \frac{e^{-\frac{1}{4} \zeta^T H_{\text{ent}} \zeta}}{\text{Tr} \left(e^{-\frac{1}{4} \zeta^T H_{\text{ent}} \zeta} \right)} = \prod_n \frac{e^{-\xi_n d_n^\dagger d_n}}{1 + e^{-\xi_n}} = \prod_n \left(\frac{1}{1 + e^{\xi_n}} d_n^\dagger d_n + \frac{1}{1 + e^{-\xi_n}} d_n d_n^\dagger \right). \quad (\text{F4})$$

This Gaussian density operator is faithfully encoded in the covariant matrix

$$\text{Tr} \left(\hat{\rho}_r i \zeta \zeta^T \right) = 2i \left(1 + e^{-H_{\text{ent}}} \right)^{-1} = \Gamma(t)_{\text{subblock}} + i, \quad (\text{F5})$$

which is just the subsystem block of the total covariant matrix $\Gamma(t)$. Therefore one can extract the eigenvalue of the disentangled density operator (occupation of the reduced canonical fermion mode) and the entanglement entropy:

$$\rho_n(t) = \frac{1}{1 + e^{\xi_n}} = \text{spec} \left\{ \frac{1 - i\Gamma(t)_{\text{subblock}}}{2} \right\}, \quad S_v(t) = - \sum_{n=1}^{N/2} (\rho_n \ln \rho_n + (1 - \rho_n) \ln (1 - \rho_n)) \leq N \ln 2/2. \quad (\text{F6})$$

The upper-bound is reached if and only if each canonical fermion is maximally entangled with a flat spectrum for the subblock of covariant matrix i.e. $\rho_n = 1/2$.

Appendix G: Turning on Majorana interaction

1. Resonant Majorana fermion interaction

The non-interacting part of the Majorana fermion Hamiltonian written in terms of spinor of local Majorana fermions can be canonical transformed to^[20]:

$$\hat{H} = \frac{1}{2} \begin{pmatrix} \alpha & \beta \end{pmatrix} H \begin{pmatrix} \alpha \\ \beta \end{pmatrix} = \frac{1}{2} \begin{pmatrix} \gamma' & \gamma'' \end{pmatrix} \tau^y \otimes \epsilon \begin{pmatrix} \gamma' \\ \gamma'' \end{pmatrix} = \begin{pmatrix} c^\dagger & c \end{pmatrix} \tau^z \otimes \epsilon \begin{pmatrix} c \\ c^\dagger \end{pmatrix}, \quad (\text{G1})$$

where $H = -H^T = -H^*$, τ^μ is the pauli matrix acting on the Nambu particle-hole spinor space, and ϵ denotes the diagonal matrix with single fermion eigenstate energy as entries. The canonical Majorana fermions γ (complex Bogoliubov fermions c) are related to the local fermions by orthogonal(unitary) matrix:

$$\begin{pmatrix} \alpha \\ \beta \end{pmatrix} = Q \begin{pmatrix} \gamma' \\ \gamma'' \end{pmatrix} = \sqrt{2} U \begin{pmatrix} c \\ c^\dagger \end{pmatrix}, \quad Q = \sqrt{2} \begin{pmatrix} \text{Re}(\psi_A) & \text{Im}(\psi_A) \\ -\text{Im}(\psi_B) & \text{Re}(\psi_B) \end{pmatrix}, \quad U = \begin{pmatrix} -i\psi_A & i\psi_A^* \\ \psi_B & \psi_B^* \end{pmatrix}, \quad (\text{G2})$$

that satisfy

$$U^\dagger H U = \begin{pmatrix} \epsilon & 0 \\ 0 & -\epsilon \end{pmatrix} \equiv \tau^z \otimes \epsilon, \quad Q^T H Q = \begin{pmatrix} 0 & -i\epsilon \\ i\epsilon & 0 \end{pmatrix} \equiv \tau^y \otimes \epsilon. \quad (\text{G3})$$

Now we bring the canonical transformation to the Majorana Hubbard interaction $\tilde{h} \sum_Y u_{i,j} u_{i,k} u_{i,l} (\beta_i \alpha_j \alpha_k \alpha_l - \alpha_i \beta_j \beta_k \beta_l)$. For convenience here we use i, j, k, l to label the spin site instead of unit-cell. Consider two inversion related Y junctions tied to the same z -link, with site labeled in counter-clockwise ordering,

$$\begin{aligned} \beta_1 \alpha_1 \alpha_2 \alpha_3 &= 4 \sum_{a,b,c,d} (\psi_{B,1,a} c_a + h.c.) (-i\psi_{A,1,b} c_b + h.c.) (-i\psi_{A,2,c} c_c + h.c.) (-i\psi_{A,3,d} c_d + h.c.) \\ &= 4 \sum_{m,n} (\text{Re}(\psi_{B,1,m}^* \psi_{A,1,m}) \text{Im}(\psi_{A,2,n}^* \psi_{A,3,n}) + \text{cycl.perm}) (2c_m^\dagger c_m - 1) (2c_n^\dagger c_n - 1) + \dots \\ &= -4 \sum_{m,n} (\text{Re}(\psi_{B,1,m}^* \psi_{A,1,m}) \text{Im}(\psi_{A,2,n}^* \psi_{A,3,n}) + \text{cycl.perm}) \gamma'_m \gamma''_m \gamma'_n \gamma''_n + \dots \end{aligned} \quad (\text{G4})$$

$$\begin{aligned} -\alpha_1 \beta_1 \beta_2 \beta_3 &= -4 \sum_{a,b,c,d} (-i\psi_{A,1,a} c_a + h.c.) (\psi_{B,1,b} c_b + h.c.) (\psi_{B,2,c} c_c + h.c.) (\psi_{B,3,d} c_d + h.c.) \\ &= 4 \sum_{m,n} (\text{Re}(\psi_{A,1,m}^* \psi_{B,1,m}) \text{Im}(\psi_{B,2,n}^* \psi_{B,3,n}) + \text{cycl.perm}) (2c_m^\dagger c_m - 1) (2c_n^\dagger c_n - 1) + \dots \\ &= -4 \sum_{m,n} (\text{Re}(\psi_{A,1,m}^* \psi_{B,1,m}) \text{Im}(\psi_{B,2,n}^* \psi_{B,3,n}) + \text{cycl.perm}) \gamma'_m \gamma''_m \gamma'_n \gamma''_n + \dots \end{aligned} \quad (\text{G5})$$

where cycl.perm denotes the cyclic permutation counterparts. One could qualitatively verify the above result by the fact that the chiral three spin interaction $\sigma_{A(B)}^x \sigma_{A(B)}^y \sigma_{A(B)}^z$ respects three-fold rotation symmetry \mathcal{C}_3 but behaves odd under either time reversal or mirror reflection symmetry

$$\begin{aligned} \mathcal{C}_3 : \sigma^{x/y/z} &\rightarrow \sigma^{y/z/x}, \quad (u, \alpha_{1/2/3}, \beta_{1/2/3}) \rightarrow (u, \alpha_{2/3/1}, \beta_{2/3/1}), \\ \mathcal{T} : \sigma^\mu &\rightarrow -\sigma^\mu, \quad (u, \alpha, \beta) \rightarrow (u, \alpha, -\beta), \quad \mathcal{M}_z : \sigma_{A/B}^{x/y/z} \rightarrow -\sigma_{B/A}^{y/x/z}, \quad (u, \alpha, \beta) \rightarrow (u, \beta, -\alpha). \end{aligned} \quad (\text{G6})$$

And \mathcal{M}_z maps $\beta_1 \alpha_1 \alpha_2 \alpha_3$ to $\alpha_1 \beta_1 \beta_2 \beta_3$, which enforces the sign difference. Inside the weight, taking the imaginary part of the wave-function overlap between the same sublattice enforces the mirror reflection odd condition. These diagonal part contributes to the leading order resonant interaction. Generally, the omitted off-diagonal terms can be Schrieffer-Wolff rotated to yield higher order correction to the resonant interaction, which usually only plays a role in exponential longer time. Here we just take the leading order term with the gauge coupling to get the symmetric interaction coupling matrix:

$$V_{m,n} = 8\tilde{h} \sum_i u_{i,j} u_{i,k} u_{i,l} \text{Re}(\psi_{i,m}^* \psi_{j,m}) \text{Im}(\psi_{k,n}^* \psi_{l,n}) + \text{cycl.perm} + (m \leftrightarrow n), \quad (\text{G7})$$

in which j, k, l are nearest neighbours arranged in counter-clockwise order surrounding site i , and i is summed over both A and B sublattices. In this way, we arrive at our final effective Hamiltonian to leading order:

$$\hat{H}_\gamma = - \sum_{n=1}^N \epsilon_n i \gamma'_n \gamma''_n - \frac{1}{4} \sum_{m,n=1}^N V_{m,n} \gamma'_m \gamma''_m \gamma'_n \gamma''_n + \dots \quad (\text{G8})$$

For completeness we here show the conserved canonical fermion parity in each random gauge configuration $\langle i \gamma'_n \gamma''_n \rangle$, and the corresponding mean-field shift of energy due to the resonant interaction, see Fig. 15.

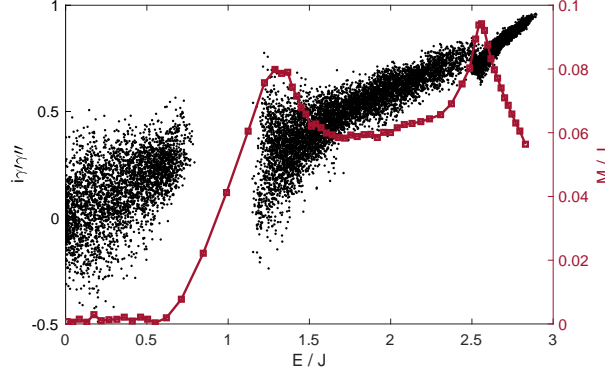


FIG. 15. Left axis: $\langle i \gamma'_n \gamma''_n \rangle$. Each dot is associated with one disordered gauge configuration. The distribution lies between the infinite temperature where $\langle i \gamma'_n \gamma''_n \rangle = 0$ and zero temperature where $\langle i \gamma'_n \gamma''_n \rangle = 1$. Right axis: mean-field energy shift $M_n \equiv \sum_m V_{m,n} \langle i \gamma'_m \gamma''_m \rangle / 4$. Parameters are $J_x = J_y = J_z = J, \hbar = 0.25J, L_x = 16, L_y = 4$, 200 disorder samples.

2. Statistics of omitted off-diagonal interaction

Here we do a statistical analysis for the off-diagonal interaction terms that were omitted. For simplicity let's fix the gauge such that nonzero gauge connection occurs only at z -link, and take a unit-cell and label the 6 sites involved as in inset of Fig. 16. The Majorana Hubbard interaction is the product of certain Majorana fermion bilinears on bonds $\hat{V} = \hbar \sum_{\text{unit-cell}} u_0 (i\alpha_0 \beta_1 i\beta_2 \beta_3 + i\alpha_0 \beta_1 i\alpha_4 \alpha_5)$, which can be straightforwardly verified by $\sigma_2^x \sigma_1^z \sigma_3^y = (\sigma_0^z \sigma_1^z) (\sigma_2^x \sigma_0^z \sigma_3^y) = (-u_0 i\alpha_0 \beta_1) (i\beta_3 \beta_2)$, likewise for $\sigma_4^x \sigma_0^z \sigma_5^y$. Using $\alpha_j = \sqrt{2} \sum_n (-i\psi_{j,n} c_n + h.c.)$, $\beta_j = \sqrt{2} \sum_n (\psi_{j,n} c_{j,n} + h.c.)$, the involved fermion bilinears can be decomposed into off-diagonal and diagonal parts:

$$\begin{aligned} i\alpha_0 \beta_1 &= \sum_{m \neq n} 2i (-i\psi_{0,m} c_m + h.c.) (\psi_{1,n} c_n + h.c.) + \sum_p 2\text{Re} (\psi_{0,p} \psi_{1,p}^*) i\gamma'_p \gamma''_p, \\ i\beta_2 \beta_3 &= \sum_{m \neq n} 2i (\psi_{2,m} c_m + h.c.) (\psi_{3,n} c_n + h.c.) + \sum_p 2\text{Im} (\psi_{2,p}^* \psi_{3,p}) i\gamma'_p \gamma''_p, \\ i\alpha_4 \alpha_5 &= \sum_{m \neq n} 2i (-i\psi_{4,m} c_m + h.c.) (-i\psi_{5,n} c_n + h.c.) + \sum_p 2\text{Im} (\psi_{4,p}^* \psi_{5,p}) i\gamma'_p \gamma''_p. \end{aligned} \quad (\text{G9})$$

A rough overview: the product of two diagonal fermion bilinears $\gamma'_p \gamma''_p \gamma'_q \gamma''_q$ contributes to the 1-bit type resonant interaction terms that have been shown previously. The product of one diagonal bilinear $\gamma'_p \gamma''_p$ and one off-diagonal bilinear $\gamma_m \gamma_n$ contributes to the off-diagonal interaction term that flips the fermion parity of two canonical fermions, which can be further decomposed into an assistant pairing term $\sim (1 - 2c_p^\dagger c_p) c_m^\dagger c_n^\dagger$ and an assistant hopping term $\sim (1 - 2c_p^\dagger c_p) c_m^\dagger c_n$, mediated by the presence or absence of other canonical fermion modes. Since the density term depending on index p is to be integrated out, the assistant pairing/hopping interaction is roughly proportional to the overlap of canonical fermion wave-function of m and n on the same given unit-cell. In contrast, the product of two off-diagonal bilinears $\gamma_m \gamma_n \gamma_p \gamma_q (m \neq n \neq p \neq q)$ that changes the fermion parity of four canonical fermion modes requires the overlap of four localized fermion wave-function on the same unit-cell, which are less dominant. In the following we do statistical analysis for the assistant hopping and pairing terms.

In detail, for the Kitaev Hamiltonian at solvable point, we sample 200 random gauge configurations $\{u_j\}$ where j labels the sites. For each gauge configuration we randomly sample 100 eigenstates, which are determined by the canonical fermion parity array $\{\nu_n\}$, with $\nu_n \equiv i \gamma'_n \gamma''_n = \pm 1$ being randomly sampled. We consider the assistant hopping(pairing) interactions connecting these random states to the target states with canonical fermion modes m, n

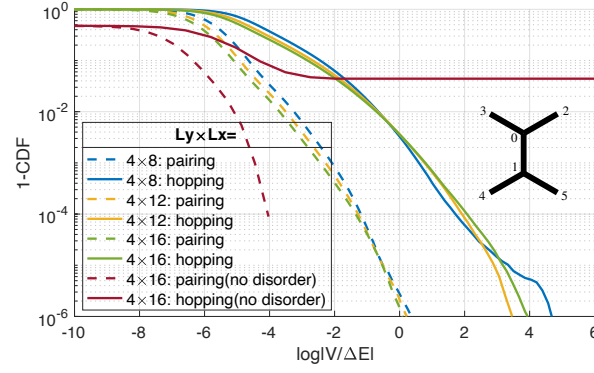


FIG. 16. Cumulative probability distribution function(CDF) for the off-diagonal interaction matrix element divided by the corresponding energy difference, in the eigenstate basis of exact solvable Hamiltonian in random gauge sectors. Varying system sizes are shown, as well as the assistant hopping and pairing types. The assistant hopping term is relatively easier to reach resonance than pairing term, with probability $\lesssim 0.5\%$. In comparison, in the zero flux sector without effective gauge flux disorder, the assistant hopping interaction shows strongly resonant contribution with $\ln|V/\Delta E| > 10^6$ with probability $\gtrsim 4\%$ among the same randomly sampled eigenstates. Therefore it is the disorder that suppresses the strong resonance. Parameters: $J_x = J_y = J_z = J, \tilde{h} = 0.25J$, sampled over 200 disorder realization of random gauge configurations, with 100 randomly sampled eigenstate in each configuration.

being flipped: $\langle \vec{\nu} - 2\nu_m \mp 2\nu_n | \hat{V} | \vec{\nu} \rangle$, for which the energy difference is $2(\epsilon_m \pm \epsilon_n)$. It can be shown that for a given choice of m, n ,

$$\langle \vec{\nu} - 2\nu_m \mp 2\nu_n | \hat{V} | \vec{\nu} \rangle = \tilde{h} \sum_p \nu_p F_{m,n,p}^\pm, \quad (\text{G10})$$

where each other inert canonical fermion mode contribute to the matrix element by a three-rank form factor tensor given by the wave-function overlap:

$$\begin{aligned} F_{m,n,p}^+ &\equiv 4 \sum_{\text{unit-cell}} \left(-iu_0 \text{Re}(\psi_{0,p} \psi_{1,p}^*) \right) \psi_{4,m}^* \psi_{5,n}^* - u_0 \text{Im}(\psi_{4,p}^* \psi_{5,p}) \psi_{0,m}^* \psi_{1,n}^* + (0 \rightarrow 4 \rightarrow 5 \rightarrow 0) \\ &\quad + iu_0 \text{Re}(\psi_{0,p} \psi_{1,p}^*) \psi_{2,m}^* \psi_{3,n}^* - u_0 \text{Im}(\psi_{2,p}^* \psi_{3,p}) \psi_{0,m}^* \psi_{1,n}^* + (1 \rightarrow 2 \rightarrow 3 \rightarrow 1) - (m \leftrightarrow n), \\ F_{m,n,p}^- &\equiv 4 \sum_{\text{unit-cell}} iu_0 \text{Re}(\psi_{0,p} \psi_{1,p}^*) \psi_{4,m}^* \psi_{5,n}^* - u_0 \text{Im}(\psi_{4,p}^* \psi_{5,p}) \psi_{0,m}^* \psi_{1,n}^* + (0 \rightarrow 4 \rightarrow 5 \rightarrow 0) \\ &\quad + iu_0 \text{Re}(\psi_{0,p} \psi_{1,p}^*) \psi_{2,m}^* \psi_{3,n}^* - u_0 \text{Im}(\psi_{2,p}^* \psi_{3,p}) \psi_{0,m}^* \psi_{1,n}^* + (1 \rightarrow 2 \rightarrow 3 \rightarrow 1) - (m \leftrightarrow n), \end{aligned} \quad (\text{G11})$$

where $(0 \rightarrow 4 \rightarrow 5 \rightarrow 0)$ and $(1 \rightarrow 2 \rightarrow 3 \rightarrow 1)$ denotes the C_3 cyclic permutation counterparts, and $(m \leftrightarrow n)$ means transposing m and n indices to enforce the anti-symmetric condition. The off-diagonal interaction matrix element divided by the energy difference serves as the strength of the first order perturbative Schrieffer-Wolff transformation generator, and therefore determines the quality of our zeroth order perturbation theory. Obtaining the interaction matrix elements for all possible $m, n = 1, \dots, N$, we calculate the cumulative probability distribution function of the logarithm of this dimensionless quantity $\ln \left| \frac{\langle \vec{\nu} | \hat{V} | \vec{\nu} \rangle}{\Delta E} \right|$, as shown in Fig. 16. The resonance condition with $\ln|V/\Delta E| \gtrsim 0$ occurs with probability $\lesssim 0.5\%$, which is the probability when our zeroth order perturbation theory would fail.

3. Correlations with dephasing interaction

In the presence of dephasing interaction, we need to transform the physical observables into the canonical fermion basis:

$$\langle D^z(t) \rangle \equiv \frac{1}{N2^N} \sum_{\{u\}} \sum_j iu_j \langle \alpha_j(t) \beta_j(t) \rangle = \frac{1}{2^N} \sum_{\{u\}} \left(\frac{1}{N} \sum_j u_j Q_{j,m} Q_{j,n} \right) \langle i\gamma_m(t) \gamma_n(t) \rangle. \quad (\text{G12})$$

The two-dimer disconnected correlation function is equivalent to the four-Majorana correlation functions as follows:

$$\begin{aligned}
C^{zz}(r, t) &\equiv \frac{1}{N} \sum_j \langle D_j^z(t) D_{j+r}^z(t) \rangle = -\frac{1}{N2^N} \sum_{\{u\}} \sum_j u_j u_{j+rn_1} \langle \alpha_j(t) \beta_j(t) \alpha_{j+rn_1}(t) \beta_{j+rn_1}(t) \rangle \\
&= -\frac{1}{N2^N} \sum_{\{u\}} \sum_j \sum_{m \neq n \neq p \neq q=1}^{2N} u_j u_{j+rn_1} Q_{j,m} Q_{j+N,n} Q_{j+rn_1,p} Q_{j+rn_1+N,q} \langle \gamma_m(t) \gamma_n(t) \gamma_p(t) \gamma_q(t) \rangle \\
&= \frac{1}{2^N} \sum_{\{u\}} \sum_{m \neq n \neq p \neq q=1}^{2N} \left(-\frac{1}{N} \sum_j u_j u_{j+rn_1} Q_{j,m} Q_{j+N,n} Q_{j+rn_1,p} Q_{j+rn_1+N,q} \right) \langle \gamma_m(t) \gamma_n(t) \gamma_p(t) \gamma_q(t) \rangle \\
&\equiv \frac{1}{2^N} \sum_{\{u\}} \sum_{m \neq n \neq p \neq q=1}^{2N} f_{m,n,p,q}^{zz} \langle \gamma_m(t) \gamma_n(t) \gamma_p(t) \gamma_q(t) \rangle = \frac{1}{2^N} \sum_{\{u\}} \sum_{m < n < p < q=1}^{2N} 24A[f_{m,n,p,q}^{zz}] \langle \gamma_m(t) \gamma_n(t) \gamma_p(t) \gamma_q(t) \rangle.
\end{aligned} \tag{G13}$$

Notice that due to the orthogonality of Q matrix $\sum_m Q_{j,m} Q_{i,m} = \delta_{i,j}$, the terms with overlapping indices drops out such that only off-diagonal Majorana correlation functions with $m \neq n \neq p \neq q$ contribute. $A[f_{m,n,p,q}^{zz}]$ means antisymmetrizing the form factor f^{zz} with respect to indices m, n, p, q , using the anticommutation relation of Majorana fermions. Likewise for $\langle D^x \rangle$ and C^{xx} .

Unlike the free fermion case, the four-point Majorana correlation function cannot be immediately factorized by Wick's theorem into simple product of two-point Majorana correlation functions. Each canonical Majorana fermion doublet $\gamma_n \equiv (\gamma'_n, \gamma''_n)^T$ is evolved effectively by a particle-hole superposition of Gaussian operators:

$$\gamma_n(t) = e^{it[H_{\text{eff}}]} \gamma_n = \sum_{\nu=\pm 1} e^{-i2t\nu\epsilon_n} e^{\frac{1}{4}\gamma^T \nu A_n \gamma} \frac{1 + \nu\tau^y}{2} \gamma_n, \quad A_n(t) \equiv -i2t(\tau^y \otimes (\oplus_j V_{n,j})). \tag{G14}$$

Then the two-point Majorana fermion correlation functions can be expressed as

$$\langle \gamma_m(t) \gamma_n(t)^T \rangle = \sum_{\mu, \nu=\pm} e^{-i2t(\mu\epsilon_m + \nu\epsilon_n)} \frac{1 + \mu\tau^y}{2} e^{-i2t\nu V_{n,m}\tau^y} \langle e^{\frac{1}{4}\gamma^T(\mu A_m + \nu A_n)\gamma} \gamma_m \gamma_n^T \rangle \frac{1 - \nu\tau^y}{2}. \tag{G15}$$

The key is to evaluate the expectation of $e^{\frac{1}{4}\gamma^T(\mu A_m + \nu A_n)\gamma} \gamma_m \gamma_n^T$ over the initial state $|\psi_{\{u\}}\rangle$. This can be generally done because the initial density matrix and the exponential operator are both Gaussian. For simplification in a given gauge configuration, we have the A sublattice absorb the neighboring gauge field on z -link $\alpha_j \rightarrow u_j \alpha_j$ such that initial state is rotated to a clean Fock vacuum, while the gauge field dependence is absorbed by $Q \rightarrow (u, 1)Q$ matrix. Turning back to the original fermion basis $\gamma^T A \gamma = \zeta^T Q A Q^T \zeta$ where $\mu A_m + \nu A_n \equiv A$ and ζ_j labels the Majorana doublet in unit-cell j , we have

$$\langle \psi_{\{u\}} | e^{\frac{1}{4}\gamma^T A \gamma} \gamma_m \gamma_n^T | \psi_{\{u\}} \rangle = \sum_{i,j} Q_{i,m} \langle \text{vac} | e^{\frac{1}{4}\zeta^T Q A Q^T \zeta} \zeta_i \zeta_j^T | \text{vac} \rangle Q_{j,n}, \tag{G16}$$

where $i\alpha_j \beta_j | \text{vac} \rangle = | \text{vac} \rangle$, and every eigenvector matrix Q has been regauged accordingly. The quantity in the middle is a vacuum expectation of the product of Gaussian operator and Majorana fermions, which can be evaluated using the generic formula that is to be derived later.

Likewise, the four-Majorana-fermion disconnected correlation function can be reduced to the expectation of the product of Gaussian operator and four Majorana fermions:

$$\begin{aligned}
\langle \gamma_m(t) \gamma_n(t) \gamma_p(t) \gamma_q(t) \rangle &= \sum_{\mu, \nu, \kappa, \lambda=\pm 1} \sum_{m', n', p', q'=1}^N e^{-i2(\mu\epsilon_m + \nu\epsilon_n + \kappa\epsilon_p + \lambda\epsilon_q)t} \\
&\times \left(\frac{1 + \mu\tau^y}{2} e^{-it2(\nu V_{n,m} + \kappa V_{p,m} + \lambda V_{q,m})\tau^y} \right)_{m,m'} \left(\frac{1 + \nu\tau^y}{2} e^{-it2(\kappa V_{p,n} + \lambda V_{q,n})\tau^y} \right)_{n,n'} \left(\frac{1 + \kappa\tau^y}{2} e^{-it2\lambda V_{q,p}\tau^y} \right)_{p,p'} \left(\frac{1 + \lambda\tau^y}{2} \right)_{q,q'} \\
&\times \langle e^{\frac{1}{4}\gamma^T(\mu A_m + \nu A_n + \kappa A_p + \lambda A_q)\gamma} \gamma_{m'} \gamma_{n'} \gamma_{p'} \gamma_{q'} \rangle.
\end{aligned} \tag{G17}$$

By denoting $\mu A_m + \nu A_n + \kappa A_p + \lambda A_q \equiv A$, we can factorize the term similarly and evaluate the effective correlation function part by Wick's theorem:

$$\langle \psi_{\{u\}} | e^{\frac{1}{4}\gamma^T A \gamma} \gamma_m \gamma_n \gamma_p \gamma_q | \psi_{\{u\}} \rangle = \langle \text{vac} | e^{\frac{1}{4}\zeta^T Q A Q^T \zeta} \gamma_m \gamma_n \gamma_p \gamma_q | \text{vac} \rangle = -Z (\tilde{\Gamma}_{m,n} \tilde{\Gamma}_{p,q} - \tilde{\Gamma}_{m,p} \tilde{\Gamma}_{n,q} + \tilde{\Gamma}_{m,q} \tilde{\Gamma}_{n,p}), \tag{G18}$$

where

$$Z \equiv \langle \text{vac} | e^{\frac{1}{4}\zeta^T Q A Q^T \zeta} | \text{vac} \rangle, \quad \tilde{\Gamma}_{m,n} \equiv \frac{\langle \text{vac} | e^{\frac{1}{4}\zeta^T Q A Q^T \zeta} \zeta_i \gamma_m \gamma_n | \text{vac} \rangle}{\langle \text{vac} | e^{\frac{1}{4}\zeta^T Q A Q^T \zeta} | \text{vac} \rangle} = \sum_{i,j} Q_{i,m} \frac{\langle \text{vac} | e^{\frac{1}{4}\zeta^T Q A Q^T \zeta} \zeta_i \zeta_j | \text{vac} \rangle}{\langle \text{vac} | e^{\frac{1}{4}\zeta^T Q A Q^T \zeta} | \text{vac} \rangle} Q_{j,n}. \tag{G19}$$

Likewise, the Loschmidt amplitude Z and the effective two-point correlation function $\tilde{\Gamma}$ can be evaluated using the general result we are going to derive in the next section.

In numerical computation, although each four-Majorana-fermion correlation function with fixed m, n, p, q reduces to effective Gaussian evolution and can be efficiently calculated, there are $\sim O(N^4)$ number of independent Gaussian evolving trajectories in total, which is a huge computation complexity to keep track of. Fortunately, it is easy for parallelization. Our computation amounts to $N = 16 \times 4$ unit-cells, which accounts for 128 spins, being averaged over 200 randomly generated disorder samples. For completeness, here we show the slices of correlation growth in fixed distances, and compare the interacting case with non-interacting case, for both isotropic coupling and anisotropic coupling respectively, see Fig. 17.

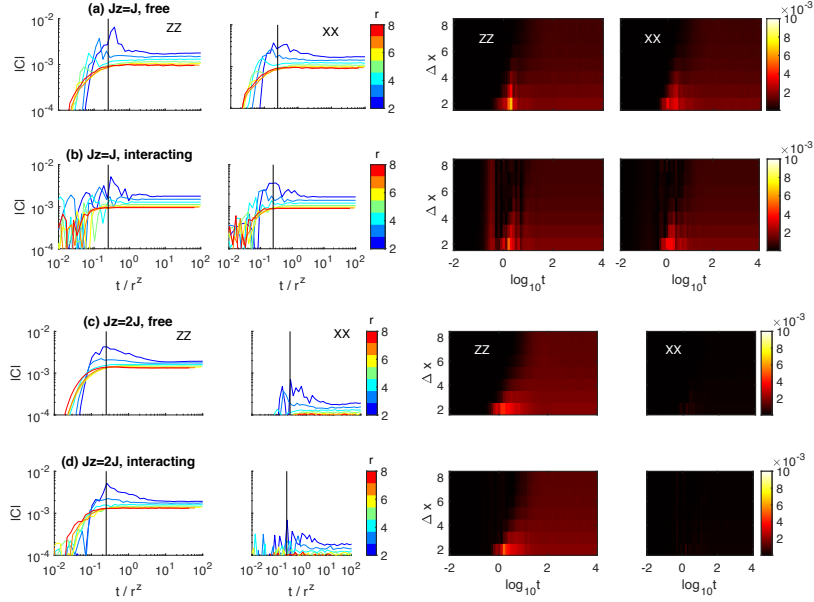


FIG. 17. Correlation growth at fixed distances and the spatiotemporal profiles. (a)(b) isotropic coupling $J_z = J_x = J_y = J, \tilde{h} = 0.25J$, using $z = 2.4$ to rescale the time axis; (c)(d) anisotropic coupling $J_z = 2J, J_x = J_y = 0.5J, \tilde{h} = 0.25J$. $L_x = 16, L_y = 4$, using $z' = 2.6$ to rescale the time axis. 10000 disorder samples for free fermion case while 200 disorder samples for the interacting scenario.

4. Extended Majorana correlation function

In this section we are going to derive an independent formula for a generic complex extended Majorana correlation function as below:

$$\langle \text{vac} | e^{\frac{1}{4}\gamma A \gamma} i \gamma \gamma^T | \text{vac} \rangle = \langle \text{vac} | e^{\frac{1}{4}\gamma A \gamma} | \text{vac} \rangle \times \frac{\langle \text{vac} | e^{\frac{1}{4}\gamma A \gamma} i \gamma \gamma^T | \text{vac} \rangle}{\langle \text{vac} | e^{\frac{1}{4}\gamma A \gamma} | \text{vac} \rangle} \equiv Z(A) \times \Gamma(A),$$

$$Z(A) = (-1)^{\frac{N(N-1)}{2}} \det(Q) \text{Pf} \left(Q^T i \tau^y Q - i \tau^y \tanh \left(\frac{a_n}{2} \right) \right) \left(\prod_n \cosh \left(\frac{a_n}{2} \right) \right), \quad \Gamma(A) = i (1 + \tau^y + (\tau^z - i \tau^x) \otimes K), \quad (\text{G20})$$

where the $|\text{vac}\rangle$ is defined by $\langle \text{vac} | i \gamma \gamma^T | \text{vac} \rangle = i(1 + \tau^y)$, γ stands for a column vector of Majorana fermion operators. The complex correlation function is factorized into a product of a Loschmidt amplitude and an effective correlation function. In general, the input argument A can be any generic complex antisymmetric matrix that has the canonical form, and K is the matrix that would appear as the Gaussian exponent coupled to the pairing term in the Balian-Brezin decomposition:

$$Q^T A Q = \tau^y \otimes (\oplus_n a_n), \quad K = \left((-i \ 1) e^A \begin{pmatrix} i \\ 1 \end{pmatrix} \right)^{-1} \left((-i \ 1) e^A \begin{pmatrix} -i \\ 1 \end{pmatrix} \right). \quad (\text{G21})$$

This formula can be applied to evaluate multiple expressions in the former section, where we turned back to the original fermion basis ζ , and regauge the initial state to be a fermion vacuum of ζ . The Pfaffian can be numerically evaluated efficiently using the algorithms and codes provided by Ref. [83].

Detailed derivation for this formula are given as follows. To evaluate the Loschmidt amplitude without sign ambiguity, we first derive a generic formula for the expectation of generic Majorana fermion Gaussian operator over the fermion vacuum, by virtue of the Baker-Campbell-Hausdorff formula for tracing out sequence of Majorana Gaussian operators as relevant in the generalized Levito's formula $\text{Tr}(e^{\frac{1}{4}\gamma A\gamma} e^{\frac{1}{4}\gamma B\gamma}) = \sqrt{\det(1 + e^A e^B)}$ [84, 85]:

$$\begin{aligned}
Z(A) &\equiv \langle \text{vac} | e^{\frac{1}{4}\gamma A\gamma} | \text{vac} \rangle = \lim_{\beta \rightarrow \infty} \text{Tr} \left(e^{-\frac{\beta}{4}\gamma\tau^y\gamma} e^{\frac{1}{4}\gamma A\gamma} \right) / \text{Tr} \left(e^{-\frac{\beta}{4}\gamma\tau^y\gamma} \right) = \lim_{\beta \rightarrow \infty} \sqrt{\det \left(\frac{1}{1 + e^{-\beta\tau^y}} + \frac{1}{1 + e^{\beta\tau^y}} e^A \right)} \\
&= \sqrt{\det \left(\frac{1 + \tau^y}{2} + \frac{1 - \tau^y}{2} e^A \right)} = \sqrt{\det \left(\frac{1 + \tau^y}{2} e^{-A/2} + \frac{1 - \tau^y}{2} e^{A/2} \right)} = \sqrt{\det \left(\cosh \left(\frac{A}{2} \right) - \tau^y \sinh \left(\frac{A}{2} \right) \right)} \\
&= \sqrt{\det \left(1 - \tau^y \tanh \left(\frac{A}{2} \right) \right)} \sqrt{\det \left(\cosh \left(\frac{A}{2} \right) \right)} = \sqrt{\det \begin{pmatrix} i\tau^y & -1 \\ 1 & i \tanh \left(\frac{A}{2} \right) \end{pmatrix}} \left(\prod_n \cosh \left(\frac{a_n}{2} \right) \right) \\
&= \text{Pf} \begin{pmatrix} i\tau^y & -1 \\ 1 & i \tanh \left(\frac{A}{2} \right) \end{pmatrix} \left(\prod_n \cosh \left(\frac{a_n}{2} \right) \right) = \text{Pf}(i\tau^y) \text{Pf} \left(i\tau^y - i \tanh \left(\frac{A}{2} \right) \right) \left(\prod_n \cosh \left(\frac{a_n}{2} \right) \right) \\
&= (-1)^{\frac{N(N-1)}{2}} \det(Q) \text{Pf} \left(Q^T i\tau^y Q - i\tau^y \tanh \left(\frac{a_n}{2} \right) \right) \left(\prod_n \cosh \left(\frac{a_n}{2} \right) \right).
\end{aligned} \tag{G22}$$

Notice that when getting rid of the square root there could be a sign factor, which is fixed to be positive in this case by analytic continuity such that $Z(A) \rightarrow 1$ when $A \rightarrow 0$, as long as $Z(A)$ remains analytic along the path of A variation and does not trespass a zone with condensed Lee-Yang-Fisher zeroes in thermodynamic limit. In finite size system, $Z(A)$ is a finite order polynomial complex function where isolated Fisher zeroes can always be avoided by infinitesimal variation. Notice that the final expression is rather complex compared to a simple $\sqrt{\det}$ at the beginning lines of derivation, but being rewritten in terms of Pfaffian has the advantage of being free from sign ambiguity [81]. Otherwise, summation over different trajectories with a sign ambiguity would lead to a sign problem like in quantum Monte Carlo calculations typically for fermion systems.

Next we derive the generic correlation matrix defined with respect to an effective Gaussian operator $|\text{vac}\rangle\langle\text{vac}| e^{\frac{1}{4}\gamma A\gamma} \equiv \lim_{\beta \rightarrow \infty} e^{-\frac{\beta}{4}\gamma\tau^y\gamma} e^{\frac{1}{4}\gamma A\gamma}$:

$$-i\Gamma(A) = \frac{\langle \text{vac} | e^{\frac{1}{4}\gamma A\gamma} \gamma \gamma^T | \text{vac} \rangle}{\langle \text{vac} | e^{\frac{1}{4}\gamma A\gamma} | \text{vac} \rangle} = \lim_{\beta \rightarrow \infty} 2(1 + e^{-\beta\tau^y} e^A)^{-1} = 2 \left(\frac{1 + \tau^y}{2} + \frac{1 - \tau^y}{2} e^A \right)^{-1} \frac{1 + \tau^y}{2}, \tag{G23}$$

by applying the general formula for correlation function $\text{Tr}(e^{\frac{1}{4}\gamma B\gamma} \gamma \gamma^T) / \text{Tr}(e^{\frac{1}{4}\gamma B\gamma}) = 2(1 + e^B)^{-1}$ which can be easily proved when B can be decomposed by orthogonal transformation to a canonical form for disentangled Majorana fermion pairs. It involves a projector that can be further simplified in the Bogoliubov-de-Gennes(BdG) basis:

$$-i\Gamma_{\text{BdG}} = -i \frac{1}{\sqrt{2}} \begin{pmatrix} i & 1 \\ -i & 1 \end{pmatrix} \Gamma \frac{1}{\sqrt{2}} \begin{pmatrix} -i & i \\ 1 & 1 \end{pmatrix} = 2 \left(\frac{1 + \tau^z}{2} + \frac{1 - \tau^z}{2} e^{A_{\text{BdG}}} \right)^{-1} \frac{1 + \tau^z}{2} = 2 \begin{pmatrix} 1 & 0 \\ -T_{22}^{-1} T_{21} & 0 \end{pmatrix}, \tag{G24}$$

where we denote $T \equiv e^{A_{\text{BdG}}}$ and the subscript labels particle-hole blocks. Notice that the above can also be directly derived by using the Balian-Brezin decomposition for $\langle \text{vac} | e^{\frac{1}{4}\gamma A\gamma} c^\dagger c^\dagger | \text{vac} \rangle = \langle \text{vac} | e^{cKc} c^\dagger c^\dagger | \text{vac} \rangle$, where the anti-symmetric matrix

$$K \equiv T_{22}^{-1} T_{21} = \left(\begin{pmatrix} -i & 1 \end{pmatrix} e^A \begin{pmatrix} i \\ 1 \end{pmatrix} \right)^{-1} \left(\begin{pmatrix} -i & 1 \end{pmatrix} e^A \begin{pmatrix} -i \\ 1 \end{pmatrix} \right). \tag{G25}$$

Turning back to the Majorana fermion basis, we have

$$-i\Gamma = 1 + \tau^y + (\tau^z - i\tau^x) \otimes K, \tag{G26}$$

that completes the derivation.

Finally we also comment that the expression above can also be consistently obtained by using the general formula of tracing out the product of two generic Gaussian operators, and the formula of the product of two Gaussian correlation functions [82] up to some further simplification. Namely, for any generic square skew-symmetric matrices A and B ,

$$\begin{aligned}
\frac{\text{Tr}(e^{\frac{1}{4}\gamma^T A\gamma} e^{\frac{1}{4}\gamma^T B\gamma})}{\text{Tr}(e^{\frac{1}{4}\gamma^T A\gamma}) \text{Tr}(e^{\frac{1}{4}\gamma^T B\gamma})} &= \frac{1}{2^{\dim(A)}} \text{Pf}(\Gamma_B) \text{Pf}(\Gamma_A + \Gamma_B^{-1}), \\
\frac{\text{Tr}(e^{\frac{1}{4}\gamma^T A\gamma} e^{\frac{1}{4}\gamma^T B\gamma} \frac{i}{2} [\gamma, \gamma^T])}{\text{Tr}(e^{\frac{1}{4}\gamma^T A\gamma} e^{\frac{1}{4}\gamma^T B\gamma})} &= 1 - (1 - \Gamma_B) \frac{1}{1 + \Gamma_A \Gamma_B} (1 - \Gamma_A), \\
\Gamma_A &= -\tanh(A/2).
\end{aligned} \tag{G27}$$

Notice that in the general formula here Γ_A is the purely skew-symmetric correlation matrix with the constant diagonal part being subtracted, slightly different from the ones we derive before.

Appendix H: Localization length in two dimensions

We use the standard free fermion method to calculate the localization length in two dimensions by scaling the quasi-1D localization length [58–60]. The first step is to put the system into a semi-infinite long stripe with fixed width L_y , and calculate the localization length for different energy $\lambda(E, L_y)$ using the transfer matrix or recursive Green's function connecting long distance. In a generic quasi 1D system, the retarded correlation connecting site 1 to far enough site x is generally expected to decay exponentially except on critical point $\|G_{1,x}\| \propto e^{-\frac{L_x}{\lambda}}$, from which one can determine the localization length λ . To reduce the rounding error, one can recursively generate the correlation function, rescaling it while recording the norm decaying rate in each step. Averaging the recorded decaying rates gives the smallest Lyapunov exponent z which is inverse proportional to the localization length λ , and since the disorder is generated in each step independently, the statistical variance of the Lyapunov exponent is accumulated:

$$\bar{z} = -\frac{1}{L_x} \sum_{x=1}^{L_x} \ln \frac{\|G_{1,x+1}\|}{\|G_{1,x}\|} \equiv \frac{1}{\lambda}, \quad \sqrt{\text{var}z} = \frac{1}{L_x} \sqrt{\sum_{x=1}^{L_x} \left(-\ln \frac{\|G_{1,x+1}\|}{\|G_{1,x}\|} \right)^2} \propto \frac{\bar{z}}{\sqrt{L_x}}, \quad (\text{H1})$$

according to the central limit theorem, given that a finite localization length exists. We'll calculate $L_y = 8, 16, 32, 64, 128$, and set the convergence threshold $\sqrt{\text{var}z}/\bar{z} \leq 0.01$ to stop the iteration. For the case that does not meet such criterion up to $L_x = 10^6$, we'll stop the iteration and let loose the threshold and keep the data with $\sqrt{\text{var}z}/\bar{z} \leq 0.1$ as tolerable. In detail, our free Majorana fermion Hamiltonian matrix is sliced into columns with intra-column and inter-column Hamiltonian coupling (using r to label the unit-cell and x to label the column, n_2 being the primitive vector along column and n_1 across columns):

$$H = \sum_x (H_x + V_{x,x+1} + V_{x,x+1}^\dagger), \quad (\text{H2})$$

$$H_x = \sum_{r_2} \begin{pmatrix} 0 & -iJ_z \\ 0 & 0 \end{pmatrix} u_r |r\rangle \langle r| + \begin{pmatrix} 0 & -iJ_x \\ 0 & 0 \end{pmatrix} |r\rangle \langle r+n_2| + \begin{pmatrix} -i\tilde{h}\tau_r & 0 \\ 0 & 0 \end{pmatrix} |r\rangle \langle r-n_2| + \begin{pmatrix} 0 & 0 \\ 0 & -i\tilde{h}\tau_r \end{pmatrix} |r\rangle \langle r+n_2| + h.c., \quad (\text{H3})$$

$$V_{x,x+1} = \sum_{r_2} \begin{pmatrix} 0 & 0 \\ iJ_y & 0 \end{pmatrix} |r\rangle \langle r-n_2| + \begin{pmatrix} -i\tilde{h} & 0 \\ 0 & i\tilde{h} \end{pmatrix} |r\rangle \langle r| + \begin{pmatrix} i\tilde{h} & 0 \\ 0 & 0 \end{pmatrix} u_r |r\rangle \langle r-n_2| + \begin{pmatrix} 0 & 0 \\ 0 & -i\tilde{h} \end{pmatrix} |r\rangle \langle r-n_2| u_{r+n_1-n_2}. \quad (\text{H4})$$

The correlation matrix connecting site 1 and site x follows from the recursive relation derived from Dyson equation

$$G_{0,x} = G_{0,x-1} V_{x-1,x} G_{x,x}, \quad G_{x,x}^{-1} = E - H_x - V_{x-1,x}^\dagger G_{x-1,x-1} V_{x-1,x}, \quad (\text{H5})$$

by initiating the left semi-infinite chain $G_{0,1} = 1, G_{1,1} = E - H_x$.

The second step is to fit the data into a one parameter scaling ansatz:

$$\frac{\lambda(E, L_y)}{L_y} = f\left(\frac{\xi(E)}{L_y}\right), \quad (\text{H6})$$

where $\xi(E)$ is the localization length we want. Numerically, this can be achieved by minimizing the variance of $\ln \xi(E) - \ln L_y$ for the interpolated data points (E, L_y) that shares identical $\lambda(E, L_y)/L_y$ [59]. The scaling function obtained by data collapse is shown as in Fig. 18.

Appendix I: Chern number in disorder

In this section we work in a typical disordered gauge configuration in the absence of fermion interaction, and resolve the localized/delocalized nature of the single-particle eigenstate wave-functions by calculating the Chern number. In a disordered configuration without translation and conservation of momentum, the Hamiltonian is no longer block diagonal in momentum space, so that the prototypical form of the TKNN Chern number formula [72] with summation over Brillouin zone can no longer be simply used. But there are in general two ways to remedy this problem.

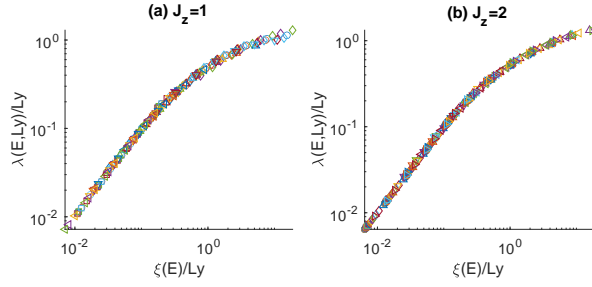


FIG. 18. Data collapse for localization length scaling function. In large width limit the scaling function is expected to approach a linear regime. (a) $J_z = J_x = J_y = J, \hbar = 0.25J, L_y = 8, 16, 32, 64, 128, L_x \leq 10^6$. (b) $J_z = 2J, J_x = J_y = 0.5J, \hbar = 0.25J, L_y = 8, 16, 32, 64, 128, L_x \leq 10^6$. Data with relative deviation of smallest Lyapunov exponent greater than 0.1 is excluded from the plot.

One way is to generalize the Brillouin zone using the concept of non-commutative geometry, which manifest in replacing summation by matrix trace in calculation, and is guaranteed to be convergent and topological if in the presence of a mobility gap [20, 61, 63]. The formula we need to calculate is

$$C = \frac{2\pi}{i} \frac{1}{N} \text{Tr}(P[[ix, P], [iy, P]]) = 2\pi i \frac{1}{N} \text{Tr}([PxP, PyP]), \quad (\text{I1})$$

where P is the spectral projector to be concretely defined below, the real space continuum coordinate operator $x(y)$ is to be expanded by the lattice coordinate in a properly defined series [62] such that the finite size error is exponentially small. Our numerical result in the main text is based on this method.

The other way is to twist the boundary phase instead [73], which takes the spirit of Laughlin's gedanken experiment of flux pumping, and can be understood as generating a super-lattice with effective quasi-momentum. In numerical calculation for a finite size lattice of discretized twisting boundary phase, it has great advantage to regularize the problem into the form of a lattice gauge theory, whose global flux over the twisting phase space is guaranteed to be quantized [74]:

$$C = \frac{1}{2\pi} \sum_{\phi} \arg \left(U_{\phi}^x U_{\phi+d\phi_x}^y U_{\phi+d\phi_y}^{x*} U_{\phi}^{y*} \right), \quad U_{\phi}^{x(y)} = \langle \psi_{\phi} | \psi_{\phi+d\phi_{x(y)}} \rangle, \quad (\text{I2})$$

where ϕ is the twisting boundary phase, $|\psi_{\phi}\rangle$ is the corresponding single particle or manybody wave-function. The other advantage of this approach is that for a free fermion problem it results in eigen-state resolved Chern numbers, from which one can determine the density of extended states [75, 77, 78], as shown in Fig. 19.

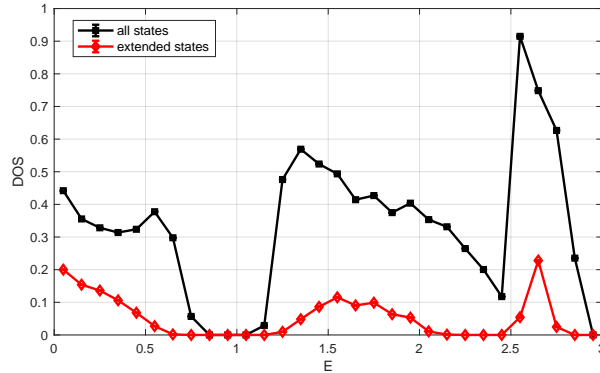


FIG. 19. Black lines: density of states from exact diagonalization in the absence of twisted phase. Red lines: density of extended single-particle states that carry nonzero Chern number, calculated in twisting boundary phase space. Parameters: $J_z = J_x = J_y = J, \hbar = 0.25J, L_x = L_y = 40, 1000$ disorder samples. Twisted phase space is discretized into 20×20 square lattice.

In the following we briefly review the technical details for these two methods. To avoid confusion, all the notations work only within the following sub-section independently and does not apply to the rest of the supplemental material.

1. Calculation using real space formula

Even without translation symmetry, one can still perform a Fourier transform and define momentum, although it is no longer good quantum number, because the single particle Hamiltonian in momentum space carries off-diagonal elements connecting different momenta. Naively, one can simply generalize the summation over momentum to matrix trace over of the spectral projector. Concretely, first let's denote the single particle spectral projector to the ground state in real space basis: $P = \frac{1 - \text{sgn}(H)}{2}$, where $\text{sgn}(H)$ is obtained by flattening the spectrum of the single particle Hamiltonian H but the sign. The spectral projector in momentum space and its derivative are

$$\tilde{P} = \frac{1}{N} e^{ik \cdot r} P e^{-ik \cdot r}, \quad \partial_k \tilde{P} = \frac{1}{N} e^{ik \cdot r} [ir, P] e^{-ik \cdot r}. \quad (I3)$$

One may generalize the Chern number formula

$$\begin{aligned} C &= \frac{1}{2\pi i} \int dk_x dk_y \text{Tr} (P(k) [\partial_{k_x} P(k), \partial_{k_y} P(k)]) \rightarrow \frac{2\pi}{i} \frac{1}{N} \text{Tr} (\tilde{P} [\partial_{k_x} \tilde{P}, \partial_{k_y} \tilde{P}]) = \frac{2\pi}{i} \frac{1}{N} \text{Tr} \left(\frac{1}{N} e^{ik \cdot r} P [[ix, P], [iy, P]] e^{-ik \cdot r} \right) \\ &= \frac{2\pi}{i} \frac{1}{N} \text{Tr} (P [[ix, P], [iy, P]]) = 2\pi i \frac{1}{N} \text{Tr} ([PxP, PyP]). \end{aligned} \quad (I4)$$

In the end, it is simply a commutator of the real space coordinate operator being projected into the Fermi sea. One could immediately verify that when $P = 1 \Rightarrow C \propto [x, y] = 0$, the contribution over the total Hilbert space is guaranteed to vanish. The essential questions are whether it converges to integer and whether it is of topological nature. First, it was elaborated early by Bellisard using the concept of non-commutative geometry [61], and later Kitaev also gave an intuitive argument for the topological nature of the 2-current of the spectral projector, and its quantization as the flow of a quasi-diagonal unitary matrix reminiscent of the Laughlin's flux pumping gedanken experiment $F(e^{i2\pi PxP}) = \text{Tr} [e^{i2\pi PxP} PyP e^{-i2\pi PxP} - PyP] / N = \int_0^{2\pi} \text{Tr} [\partial_\phi e^{i\phi [PxP]} PyP] d\phi / N = 2\pi i [PxP, PyP] / N$ [20]. Note that the quasi-diagonal condition of the unitary matrix is readily satisfied when there is a spectral or mobility gap so that correlation exponentially decays. Note also that Bianco et.al. also derived a similar formula from the linear response theory for continuum real space system [63], and they even took out the local contribution in each unit-cell i.e. the diagonal entry of the commutator $2\pi i [PxP, PyP]$ and defined a so-called local Chern marker, which in a clean system is equivalent to the total Chern number. However, one should notice that the trade of k -derivative with commutator of coordinate $\partial_k \rightarrow [ir, \cdot]$ is exact only at thermodynamic limit $N \rightarrow \infty$ such that $\Delta k \rightarrow 0$ can be infinitesimally small. Prodan et.al. proposed an efficient numerical algorithm to exponentially suppress the finite size error in this line as follows [62]. In a finite size system with L units along x -direction, one could approximate the real-space coordinate by an expansion $x \simeq \sum_{n=1}^{L/2} a_n (e^{in \frac{2\pi}{L} x} - c.c.)$. As what we need is not to cover the whole lattice coordinate, but to approach the continuum limit of small x , a direct discrete Fourier transform for the lattice coordinate is apparently not the optimal choice, which yields polynomial $O(1/L^2)$ error. One optimal solution is chosen by solving the linear matrix equation $\sum_{n=1}^{L/2} a_n n^{2j-1} = \frac{L}{2\pi} \delta_{j,1}$, ($j = 1, \dots, L/2$) such that the deviation between the continuous x and the expanded series is exactly 0 up to $L/2$ -th order, leading to exponentially small error with the system size: $O(\frac{1}{L})^L$. As coordinate operator generates the translation of momentum, we have

$$[ix, P] = e^{-ik \cdot r} (\partial_k \tilde{P}) e^{ik \cdot r} = \sum_{n=1}^{L/2} a_n \left(e^{i \frac{2\pi}{L} n \cdot r} P e^{-i \frac{2\pi}{L} n \cdot r} - e^{-i \frac{2\pi}{L} n \cdot r} P e^{i \frac{2\pi}{L} n \cdot r} \right) + O\left(\frac{1}{L}\right)^L. \quad (I5)$$

2. Calculation by twisting boundary phase

It is akin to the momentum space formula for the Chern number [72, 73, 77]. By discretizing the twisted boundary phase space into $M_x \times M_y$ sites, it is equivalent to treat the $L_x \times L_y$ finite-size system as a giant unit-cell and generate a periodic super-lattice of size $L_x \times L_y \times M_x \times M_y$, thus effectively generating a mini-Brillouin-zone(BZ) for the quasi-momentum in unit of $2\pi / M_{x(y)}$. In the mini-BZ, the $L_x \times L_y$ large unit cell folds into $L_x \times L_y$ mini-bands. Since the twisting phase ϕ , conjugate to the real space coordinate, plays the role of a quasi-momentum ranging between $[0, 2\pi/L]$ [73]:

$$C = \frac{1}{2\pi i} \int_{\partial \text{BZ}} d\vec{\phi} \cdot \langle \psi | \partial \psi \rangle = \frac{1}{2\pi} \int_{\text{BZ}} d\phi_x d\phi_y F_\phi, \quad F_\phi = i \langle \partial_{\phi_x} \psi(\phi) | \partial_{\phi_y} \psi(\phi) \rangle + h.c. \quad (I6)$$

where $\psi(\phi)$ can either be the single particle eigenstate or manybody eigenstate for the Hamiltonian with twisting boundary phase ϕ . Physically, the twisting boundary phase also concurs with Laughlin's flux pumping gedanken

experiment. In a finite-size lattice system, one could regularize the above formula like regularizing the continuum gauge theory into a lattice gauge theory [74]. Namely, regularize the local flux integrated over a plaquette as the Wilson loop of the $U(1)$ link variable, which is physically the parallel transportation of the wave-function:

$$C = \frac{1}{2\pi} \sum_{\phi} \arg \left(U_{\phi}^x U_{\phi+d\phi_x}^y U_{\phi+d\phi_y}^{x*} U_{\phi}^{y*} \right), \quad U_{\phi}^{x(y)} = \langle \psi_{\phi} | \psi_{\phi+d\phi_{x(y)}} \rangle. \quad (\text{I7})$$

where \arg is defined as taking the phase angle from the principal branch $(-\pi, \pi]$. Notice that the parallel transporter circulating the BZ should be equivalent to identity due to the periodicity (close manifold without boundary), which means the total flux must be quantized in units of 2π , therefore guaranteeing the quantization of Chern number defined on this lattice. Whether this global flux coincides with the continuum limit is a question. While there is no limitation to the flux on each plaquette in the continuum limit as a noncompact gauge theory, there is 2π ambiguity of flux on each plaquette in the lattice gauge theory with compact gauge group. This is the source of the discrepancy between the lattice and the continuum limit. Generally, when the phase grid of the lattice is fine enough such that the corresponding flux on each plaquette in continuum limit is controlled within the principal branch window, the finite size result should unambiguously concurs with the continuum limit. Assuming a smooth Berry curvature configuration, by uniformly distributing the Berry flux onto each plaquette approximately, one can estimate a lower-bound for the required size of the phase space: $M_x M_y > 2|C|$. As we know, for a low-energy Dirac fermion with light mass, the Berry curvature is sharply peaked around the Dirac point, but the distribution is flattened when the mass is large.

The quantization of Chern number in continuum limit relies on the adiabatic evolution of the ground state wave-function circulating around the twisting phase space. In other words, it also requires a mobility gap at the Fermi-level, or a (exponentially) fast decay of the correlation function, which excludes the situation with Fermi-level crossing a band in a clean system. In cases with band overlapping or level crossing, the Berry curvature could have singularity. However, in a generally disordered finite size system, this generally holds because either the states near Fermi-level is localized without contribution to Berry curvature, or the delocalized states near Fermi-level are generally experiencing level repulsion due to scattering. Notice that the Bloch state in clean system without momentum scattering and manybody interaction is a very special case in this sense.

In practice, one can either use the manybody ground state (such as the Slater determinant for free fermion system) to construct the link variable, or resolve the Berry phase for each single particle eigen-state, which gives biproduct of determining the localization nature of a wave-function [75, 77]. Further, one can perform scaling analysis for the density of extended states versus the total states to deduce the existence of extended states in thermodynamic limit that escapes localization [78].

Appendix J: Zero energy thermal metallic state

In this section we show numerical verification for the delocalized nature of the single particle mode at zero energy for the isotropic coupling model for larger system size, which is qualitatively consistent with the infinite temperature limit of a moderate size numerical calculations in Ref. [69]. To resolve the density of states at extremely small energy, we use the standard kernel polynomial method [70], to expand the density of states, defined as a collection of δ functions, in the orthogonal basis of Chebyshev polynomials,

$$\rho(E) = \frac{1}{\pi \sqrt{1 - (E/E_{\max})^2}} \left(1 + 2 \sum_{n=1}^{\infty} \text{Tr}(T_n(H/E_{\max})) T_n(E/E_{\max}) \right). \quad (\text{J1})$$

where T_n is the first kind of Chebyshev polynomials, and the coefficient at each order can be evaluated iteratively in terms of sparse matrix. 10 random complex states are initiated to evaluate the trace of matrix stochastically. In this way we can go to very large system size with finer energy resolution. When truncated at finite orders, a Jackson kernel is attached to damp the Gibbs oscillations, resulting in a smooth regular function. Results are shown in Fig. 20ab. A logarithmic divergent behaviour close to zero energy is visible, consistent with the theoretical prediction [65].

To verify the weak multi-fractal nature of the single fermion wave-function at zero energy, we first look at the fractal dimension of the generalized inverse participation ratio [76]:

$$D_q = \frac{1}{1-q} \frac{\ln \sum_r p(r)^q}{\ln L}, \quad (\text{J2})$$

where $p(r) \equiv |\psi(r)|^2$ is the zero energy single particle wave-function probability distribution, L is the coarse grained linear system size. In practical numerical calculation, to reduce the interference of the lattice length scale, we typically do a coarse graining for $p(r)$, where r is the coarse grained coordinate. To calculate the singularity spectrum $f(\alpha)$

that is related to D_q by the Legendre transform $D_q(1-q) = f(\alpha) - \alpha q$, $f'(\alpha) = q$, we first define a set of normalized weight $\mu_q(r) = p(r)^q / \sum_r p(r)^q$. Then the scaling dimension of q -th moment weighted average probability, and the associated volume scaling dimension are respectively given by

$$\alpha(q) = \frac{\sum_r \mu_q(r) \ln p(r)}{-\ln L}, \quad f(\alpha(q)) = \frac{\sum_r \mu_q(r) \ln \mu_q(r)}{-\ln L}. \quad (\text{J3})$$

It can be checked that $f(\alpha(q=0)) = 2$. Similar to a $2+\epsilon$ dimensional metal near the Anderson localization, our results show weak multi-fractal behaviour $D_q = 2 - \gamma q$, when $\gamma q \ll 2$, and $\alpha(q=0) = d - \gamma$, as shown in Fig. 20cd.

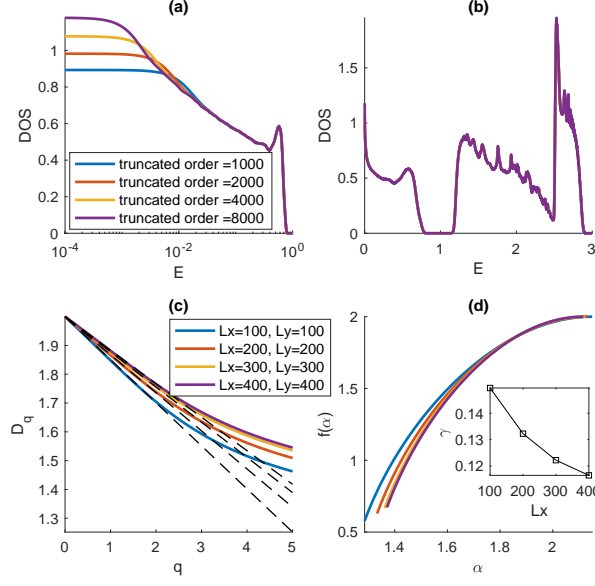


FIG. 20. (a)(b) Density of states (DOS) calculated using kernel polynomial method with different truncated orders. $L_x = L_y = 100$. The large scale DOS is consistent with the exact diagonalization result in Fig. 19. (c) Fractal dimensions of the generalized inverse participation ratio defined out of q -th moment of zero energy single particle wave-function probability distribution. Dashed lines sketch the weak multifractal behaviour: $D_q = 2 - \gamma q$. (d) Singular spectrum of wave-function intensity distribution. Inset shows the finite size dependence of γ . Parameters: $J_z = J_x = J_y = J$, $\hbar = 0.25J$.